

## Pulsar-timing arrays, astrometry, and gravitational waves

Wenzer Qin,<sup>1</sup> Kimberly K. Boddy,<sup>1</sup> Marc Kamionkowski,<sup>1</sup> and Liang Dai<sup>2</sup>

<sup>1</sup>*Department of Physics and Astronomy, Johns Hopkins University,  
3400 N. Charles St., Baltimore, Maryland 21218, USA*

<sup>2</sup>*School of Natural Sciences, Institute for Advanced Study, Princeton, New Jersey 08540, USA*



(Received 17 October 2018; published 5 March 2019)

We discuss the theory of pulsar-timing and astrometry probes of a stochastic gravitational-wave background with a recently developed “total-angular-momentum” (TAM) formalism for cosmological perturbations. We review the formalism, emphasizing in particular the features relevant for this work and describe the observables we consider (i.e., the pulsar redshift and stellar angular displacement). Using the TAM approach, we calculate the angular power spectra for the observables and from them derive angular auto- and cross-correlation functions. We provide the full set of power spectra and correlation functions not only for the standard transverse-traceless propagating degrees of freedom in general relativity, but also for the four additional non-Einsteinian polarizations that may arise in alternative-gravity theories. We discuss how pulsar-timing and astrometry surveys can complement and serve as cross checks to one another and comment on the importance of testing the chirality of the gravitational-wave background as a tool to understand the nature of its sources. A simple rederivation of the power spectra from the plane-wave formalism is provided in an Appendix.

DOI: [10.1103/PhysRevD.99.063002](https://doi.org/10.1103/PhysRevD.99.063002)

### I. INTRODUCTION

Efforts to detect a stochastic gravitational-wave background using pulsar-timing arrays have been around for almost three decades [1]. There are now three major efforts: the Parkes Pulsar Timing Array [2,3], North American Nanohertz Observatory for Gravitational Waves [4], and the European Pulsar Timing Array [5]. The three collaborate through an International Pulsar Timing Array (IPTA) [6]. The effects of gravitational waves on the pulse arrival times from pulsars were worked out presciently first in Refs. [7,8]. The signature of a stochastic gravitational-wave background is the characteristic angular correlation in the timing residuals worked out by Hellings and Downs [9]. The measurements, which span timescales of years, are sensitive primarily to gravitational waves with frequencies  $\sim 10^{-9} \text{ sec}^{-1}$ , though constraints at lower frequencies have been considered as well [10]. The endeavor is particularly exciting given that a stochastic background in this frequency range is expected from the mergers of supermassive-black-hole binaries [11–15]. The first data release from IPTA has placed a  $2\sigma$  limit on the dimensionless strain of the stochastic background to be  $1.7 \times 10^{-15}$  at a frequency of  $1 \text{ yr}^{-1}$ , with an assumed spectral index of  $-2/3$ , and significant improvement in sensitivity is expected with the next dataset [6]. See Refs. [16–20] for recent reviews of the effort to detect gravitational waves with pulsar timing.

Attention has recently turned to the possibility to detect a stochastic gravitational-wave background with astrometry [21,22], which probes frequencies  $H_0 \lesssim f \lesssim 1 \text{ yr}^{-1}$

( $10^{-18} \text{ s}^{-1} \lesssim f \lesssim 10^{-8} \text{ s}^{-1}$ ) that overlap with and bridge the frequency gap between cosmic microwave background polarization measurements and pulsar-timing measurements [23]. Book and Flanagan [24] provided the first detailed characterization of the expected signals in terms of angular correlation functions and power spectra. Their work has been extended to the search for point sources of gravitational waves [25] and to non-Einsteinian polarizations [26,27], the latter of which echoes analogous work for pulsar timing [28,29]. Astrometric data from GAIA and extragalactic radio sources constrain the energy density (integrated over  $\ln f$ ) of the stochastic background to be  $< 0.011$  for frequencies  $6 \times 10^{-18} \text{ s}^{-1} \lesssim f \lesssim 10^{-9} \text{ s}^{-1}$  [23]. Future astrometry missions [30] might provide improved data for such measurements.

Here we extend previous work on the calculation of angular correlation functions and angular power spectra for pulsar-timing and astrometry probes of the gravitational-wave background by employing a “total-angular-momentum” (TAM) formalism developed recently [31,32] for the study of cosmological perturbations. In most discussions of cosmological perturbations and stochastic gravitational-wave backgrounds, the spacetime-metric perturbation is decomposed into plane waves  $e^{ik \cdot x}$ , as these provide a simple and familiar complete orthonormal basis. For gravitational waves in general relativity, there are two polarizations, typically taken to be  $+$  and  $\times$ , with polarization vectors  $\epsilon_{ab}^+(\mathbf{k})$  and  $\epsilon_{ab}^\times(\mathbf{k})$  associated with each wave vector  $\mathbf{k}$ . The simplicity is lost, though, when projecting

these plane waves onto observables on the spherical sky. The TAM approach has been applied to simplify calculations of weak gravitational lensing [31], angular three-point functions [32], and circular polarization of the cosmic microwave background [33].

As elaborated below, the TAM formalism provides an alternative complete orthonormal set of basis functions: the TAM waves. In this formalism, the wave vector  $\mathbf{k}$  is replaced by quantum numbers  $k\ell m$ , where  $k$  is a wave number magnitude (equivalent to  $|\mathbf{k}|$ ) and  $\ell m$  are total-angular-momentum quantum numbers. Observables on the sphere are similarly quantified in terms of quantum numbers  $\ell m$ , and any such observable receives contributions only from TAM waves of the same  $\ell m$ . This leads, as we will see, to simple derivations of the predictions for harmonic-space observables. The  $+$  and  $\times$  polarizations in the plane-wave expansion are replaced in TAM waves by two transverse-tensor polarizations which we call “tensor E” (TE) and “tensor B” (TB). We decompose the two scalar polarizations that may arise in alternative-gravity theories into scalar-transverse (ST), sometimes referred to as “breathing,” and scalar-longitudinal (SL) modes to correspond to the decomposition used in prior work. There are also two vector polarizations that we call “vector E” (VE) and “vector B” (VB).

Our paper is organized as follows: in Sec. II we first describe our characterization of the observables. For pulsar timing, this is pulse frequency, and for astrometry the angular positions, at two different epochs. These are then translated to spherical-harmonic coefficients from which correlation functions and power spectra are derived. We provide the complete set of six two-point angular correlation (and cross-correlation) functions for a combined pulsar-timing/astrometry survey and relate them to the six angular power spectra. We summarize briefly our main results in Sec. III before going through the calculations in Sec. IV, first for the redshift and then for astrometry. This section also discusses the results for the various power spectra and autocorrelation functions. Section V presents results for the redshift-astrometry cross-correlations. In Sec. VI we discuss the range of gravitational-wave frequencies probed by pulsar timing and astrometry, point out that information on the local three-dimensional metric perturbation can be reconstructed from combined angular/time-sequence information, and emphasize the importance of pursuing the parity-violating observables that may arise from chirality in the gravitational-wave background. Section VII provides concluding remarks. In Appendix A we provide a brief reprise of Ref. [31], emphasizing in particular the aspects relevant for the study of a stochastic gravitational-wave background, as well as a few new results needed for our calculations. Appendix B provides some Legendre-polynomial relations needed to translate angular power spectra and angular correlation functions. Appendix C describes a simple alternative technique, based on the

plane-wave formalism, to derive all of the power-spectrum results. Appendix D derives the relations between angular power spectra and correlation functions.

## II. OBSERVABLES

We begin by describing the observables. For simplicity/clarity, we assume that there are PTA and astrometry measurements performed at two times  $t$  and  $t + \Delta t$  separated by a time interval  $\Delta t$ . The generalization to more realistic observational cadences is described briefly later.

### A. Spherical-harmonic coefficients and power spectra

We assume a multitude of pulsars spread throughout the sky and that a pulsar in a direction  $\hat{\mathbf{n}}$  is observed to have a redshift  $z(\hat{\mathbf{n}}, t)$  at time  $t$ . Since, in practice, a single pulse is typically buried in noise and is thus undetectable, the relevant observable is the timing residual  $\int^t dt' z(\hat{\mathbf{n}}, t')$ , obtained by accumulating many pulses. To simplify the discussion in this paper, we consider the observable to be the change  $(\delta z)(\hat{\mathbf{n}}, t) \equiv z(\hat{\mathbf{n}}, t + \Delta t) - z(\hat{\mathbf{n}}, t)$  over the time interval  $\Delta t$ .<sup>1</sup> These observational “data” can be represented alternatively and equivalently in terms of the spherical-harmonic coefficients,

$$z_{\ell m}(t) = \int d\hat{\mathbf{n}} Y_{\ell m}^*(\hat{\mathbf{n}}) (\delta z)(\hat{\mathbf{n}}, t), \quad (1)$$

where  $Y_{\ell m}(\hat{\mathbf{n}})$  are spherical harmonics. If the  $z_{\ell m}(t)$  are provided, the change in redshift can be obtained from the inverse transformation,

$$(\delta z)(\hat{\mathbf{n}}, t) = \sum_{\ell=0}^{\infty} \sum_{m=-\ell}^{\ell} z_{\ell m}(t) Y_{\ell m}(\hat{\mathbf{n}}). \quad (2)$$

For astrometry measurements, we assume that each source, with its proper motion already accounted for, in the survey has moved an angular distance  $(\delta n)_a$  over the time interval  $\Delta t$  due to the presence of a gravitational-wave background. From such measurements for sources spread over the sky, we obtain a deflection-angle field  $(\delta n)_a(\hat{\mathbf{n}})$ , which is a vector field (represented with the single abstract index  $a$ ) that lives in the celestial sphere and is a function of position on the sky. It can thus be expanded in vector spherical harmonics [as defined in Eq. (38) in Ref. [31]],<sup>2</sup>

$$(\delta n)_a(\hat{\mathbf{n}}) = \sum_{lm} [E_{\ell m} Y_{(\ell m)a}^E(\hat{\mathbf{n}}) + B_{\ell m} Y_{(\ell m)a}^B(\hat{\mathbf{n}})], \quad (3)$$

<sup>1</sup>Using the simplified observable  $(\delta z)(\hat{\mathbf{n}}, t)$  does not affect our main results, which relate to the angular dependence of correlation functions.

<sup>2</sup>Appendix B in Ref. [34] provides useful properties of these harmonics, although their vector harmonics are smaller than ours by a factor of  $\sqrt{2}$ .

in terms of spherical-harmonic coefficients,

$$\begin{aligned} E_{\ell m} &= \int d\hat{n} (\delta n)^a(\hat{n}) Y_{(\ell m)a}^E(\hat{n}), \\ B_{\ell m} &= \int d\hat{n} (\delta n)^a(\hat{n}) Y_{(\ell m)a}^B(\hat{n}). \end{aligned} \quad (4)$$

The values that the  $z_{\ell m}$ ,  $E_{\ell m}$ , and  $B_{\ell m}$  take depend on how our coordinate system is chosen. The power spectra

$$C_{\ell}^{XX} = \frac{1}{2\ell + 1} \sum_m |X_{\ell m}|^2, \quad (5)$$

for  $X = \{z, E, B\}$  are, on the other hand, rotational invariants. Here  $C_{\ell}^{EE}$  and  $C_{\ell}^{BB}$  are power spectra for, respectively, the E and B modes. There are three additional cross-correlation power spectra,

$$C_{\ell}^{XX'} = \frac{1}{2\ell + 1} \sum_m X_{\ell m} (X'_{\ell m})^*, \quad (6)$$

for  $XX' = \{zE, zB, EB\}$  that are also rotationally invariant. The cross-spectrum  $C_{\ell}^{EB}$  is expected, given the opposite parities of E and B, to be zero unless the gravitational-wave background breaks parity. The redshift  $z(\hat{n}, t)$  is associated with the longitudinal vector harmonic, which has the same parity as E. Thus, we also expect  $C_{\ell}^{zB}$  to be zero and  $C_{\ell}^{zE}$  to be nonzero if parity is not broken.

If the signal is due to a statistically isotropic stochastic background, then we expect

$$\langle X_{\ell m} (X'_{\ell' m'})^* \rangle = C_{\ell}^{XX'} \delta_{\ell\ell'} \delta_{mm'}, \quad (7)$$

for all six  $XX' = \{zz, EE, BB, zE, zB, EB\}$ . This expression says that the variance of any  $X_{\ell m}$  is  $C_{\ell}^{XX}$ , and the covariance of any two different ones is  $C_{\ell}^{XX'}$ . It also tells us that each spherical-harmonic coefficient is statistically independent. If the background is moreover a Gaussian random field (e.g., as arises for inflationary gravitational waves), then each  $X_{\ell m}$  (actually, its real and imaginary components) is chosen from a Gaussian distribution. In this case, the variance with which the theoretical expectation for  $C_{\ell}^{XX}$  can be obtained in the ideal case is  $\sqrt{2/(2\ell + 1)} C_{\ell}^{XX}$  (with analogous expressions for the covariances as given, for example, in Ref. [35]). In practice, the most likely background, from supermassive black holes (SMBHs), is unlikely to be Gaussian, and so this cosmic variance will be a bit different [36,37].

The statistical independence of the  $X_{\ell m}$  gives the harmonic approach (i.e., working with the  $X_{\ell m}$  and  $C_{\ell}^{XX'}$ ) a conceptual advantage over the configuration-space approach [i.e., working with  $(\delta z)(\hat{n})$  and  $(\delta n)^a(\hat{n})$ ]. The advantage may not be so clear in practice, though, given the potentially limited number of pulsars or stellar sources or

their irregular distribution in the sky. If the local stochastic background is dominated by the signal from a handful of nearby sources, then the background will be non-Gaussian and depart from statistical isotropy. This, too, compromises the conceptual advantage of the  $X_{\ell m}$  over the configuration-space description. For these reasons, it is beneficial to have at hand also a description of the correlations in terms of real-space correlation functions, to which we now turn.

### 1. Correlation functions

The angular two-point autocorrelation function for the redshift is

$$\begin{aligned} C^{zz}(\Theta) &\equiv \langle (\delta z)(\hat{n})(\delta z)(\hat{m}) \rangle_{\hat{n}\cdot\hat{m}=\cos\Theta} \\ &= \sum_{\ell} \frac{2\ell + 1}{4\pi} C_{\ell}^{zz} P_{\ell}(\cos\Theta), \end{aligned} \quad (8)$$

where  $P_{\ell}(\cos\Theta)$  are Legendre polynomials and the angle brackets denote an average over all pairs of points separated by an angle  $\Theta$ . This (as we will rederive below) is given by the Hellings-Down curve for an isotropic stochastic background of transverse-traceless gravitational waves.

Rotationally invariant correlation functions for the angular deflection can be written in terms of the scalar functions  $E(\hat{n})$  and  $B(\hat{n})$ , obtained by taking the divergence and curl, respectively, of the vector field; these are the correlation functions  $\beta^{EE}(\Theta)$  and  $\beta^{BB}(\Theta)$  in Ref. [24] and the  $EE(\Theta)$  and  $BB(\Theta)$  functions in Ref. [27]. Although well-defined mathematically, these scalars can only be computed from a smooth full-sky map and are unstable to reconstruction errors. We therefore work instead (as have prior authors [24,26,27]) with rotationally invariant correlation functions for vector fields (following the analogous approach in Ref. [35] for tensor fields).

Consider the correlation of a vector field  $(\delta n)^a(\hat{n})$  at a point  $\hat{n}$  on the sky with a value  $(\delta n)^a(\hat{m})$  at another point  $\hat{m}$ . We can then consider the great arc connecting these two points on the sphere and then write these vectors in terms of components  $(\delta n)^{\parallel}$  and  $(\delta n)^{\perp}$  that are parallel and perpendicular, respectively, to that great arc. There are then two autocorrelations,

$$\begin{aligned} C^{\parallel\parallel}(\Theta) &= \langle (\delta n)^{\parallel}(\hat{n})(\delta n)^{\parallel}(\hat{m}) \rangle_{\hat{n}\cdot\hat{m}=\cos\Theta}, \\ C^{\perp\perp}(\Theta) &= \langle (\delta n)^{\perp}(\hat{n})(\delta n)^{\perp}(\hat{m}) \rangle_{\hat{n}\cdot\hat{m}=\cos\Theta}, \end{aligned} \quad (9)$$

and also a cross-correlation,

$$C^{\perp\parallel}(\Theta) = \langle (\delta n)^{\perp}(\hat{n})(\delta n)^{\parallel}(\hat{m}) \rangle_{\hat{n}\cdot\hat{m}=\cos\Theta}, \quad (10)$$

that is nonzero only if parity is somehow broken (i.e., if  $C_{\ell}^{EB} \neq 0$ ). There are also two angular cross-correlation functions,

$$\begin{aligned} C^{\parallel}(\Theta) &= \langle (\delta z)(\hat{n})(\delta n)^{\parallel}(\hat{m}) \rangle_{\hat{n}\cdot\hat{m}=\cos\Theta}, \\ C^{\perp}(\Theta) &= \langle (\delta z)(\hat{n})(\delta n)^{\perp}(\hat{m}) \rangle_{\hat{n}\cdot\hat{m}=\cos\Theta}, \end{aligned} \quad (11)$$

between the redshift and the two components of the deflection angle aligned with the great arc connecting the points being correlated. Again, the latter of these vanishes if there is no parity breaking (i.e., if  $C_{\ell}^{zB} = 0$ ). To summarize, there are, for the combined astrometry/pulsar-timing survey, six correlation functions ( $\parallel\parallel$ ,  $\perp\perp$ ,  $z\perp$ ,  $\perp\perp$ ,  $z\parallel$ , and  $z\perp$ ).

The six sets of correlation functions contain the same information as the six sets of power spectra. They are related to the power spectra through [in addition to Eq. (8)]

$$C^{\parallel\parallel}(\Theta) = \sum_{\ell} \frac{2\ell+1}{4\pi} [C_{\ell}^{EE} G_{(\ell_1)}(\Theta) + C_{\ell}^{BB} G_{(\ell_2)}(\Theta)], \quad (12)$$

$$C^{\perp\perp}(\Theta) = \sum_{\ell} \frac{2\ell+1}{4\pi} [C_{\ell}^{EE} G_{(\ell_2)}(\Theta) + C_{\ell}^{BB} G_{(\ell_1)}(\Theta)], \quad (13)$$

$$\begin{aligned} C^{z\parallel}(\Theta) &= \sum_{\ell} \sqrt{\frac{2\ell+1}{4\pi}} C_{\ell}^{zE} Y_{(\ell_1)}(\Theta, 0) \\ &= \sum_{\ell} \frac{2\ell+1}{4\pi} \frac{1}{\sqrt{\ell(\ell+1)}} C_{\ell}^{zE} P_{\ell}^1(\cos\Theta), \end{aligned} \quad (14)$$

$$\begin{aligned} C^{z\perp}(\Theta) &= \sum_{\ell} \sqrt{\frac{2\ell+1}{4\pi}} C_{\ell}^{zB} Y_{(\ell_1)}(\Theta, 0) \\ &= \sum_{\ell} \frac{2\ell+1}{4\pi} \frac{1}{\sqrt{\ell(\ell+1)}} C_{\ell}^{zB} P_{\ell}^1(\cos\Theta), \end{aligned} \quad (15)$$

$$C^{\perp\parallel}(\Theta) = \sum_{\ell} \frac{2\ell+1}{4\pi} C_{\ell}^{EB} [G_{(\ell_1)}(\Theta) - G_{(\ell_2)}(\Theta)], \quad (16)$$

where

$$\begin{aligned} G_{(\ell_1)}(\Theta) &\equiv -\frac{1}{2} \left[ \frac{1}{\ell(\ell+1)} P_{\ell}^2(\cos\Theta) - P_{\ell}^0(\cos\Theta) \right], \\ G_{(\ell_2)}(\Theta) &\equiv -\frac{1}{\ell(\ell+1)} \frac{P_{\ell}^1(\cos\Theta)}{\sin\Theta}, \end{aligned} \quad (17)$$

and  $P_{\ell}^m(\cos\Theta)$  are associated Legendre polynomials.

The inverse of these relations are

$$C_{\ell}^{zz} = 2\pi \int_{-1}^1 d\cos\Theta C^{zz}(\Theta) P_{\ell}(\cos\Theta), \quad (18)$$

$$\begin{aligned} C_{\ell}^{EE} &= 2\pi \int_{-1}^1 d\cos\Theta [C^{\parallel\parallel}(\Theta) G_{(\ell_1)}(\Theta) \\ &\quad - C^{\perp\perp}(\Theta) G_{(\ell_2)}(\Theta)], \end{aligned} \quad (19)$$

$$\begin{aligned} C_{\ell}^{BB} &= 2\pi \int_{-1}^1 d\cos\Theta [-C^{\parallel\parallel}(\Theta) G_{(\ell_2)}(\Theta) \\ &\quad + C^{\perp\perp}(\Theta) G_{(\ell_1)}(\Theta)], \end{aligned} \quad (20)$$

$$C_{\ell}^{EB} = 2\pi \int_{-1}^1 d\cos\Theta C^{\perp\parallel} [G_{(\ell_1)}(\Theta) + G_{(\ell_2)}(\Theta)] \quad (21)$$

$$\begin{aligned} C_{\ell}^{zE} &= \frac{2\pi}{\sqrt{\ell(\ell+1)}} \int_{-1}^1 d\cos\Theta C^{z\parallel}(\Theta) P_{\ell}^1(\cos\Theta), \\ C_{\ell}^{zB} &= \frac{2\pi}{\sqrt{\ell(\ell+1)}} \int_{-1}^1 d\cos\Theta C^{z\perp}(\Theta) P_{\ell}^1(\cos\Theta). \end{aligned} \quad (22)$$

Appendix D derives these relations.

### III. PREDICTIONS FOR POWER SPECTRA: SUMMARY OF RESULTS

We now provide results for the six power spectra  $C_{\ell}^{XX'}$ . We provide these results for each of the six possible gravitational-wave polarizations. As we will see, all of our results (except for those for the longitudinal polarization, about which we will say more below) appear in the form,

$$\begin{aligned} C_{\ell}^{XX',\alpha} &= 32\pi^2 F_{\ell}^{X,\alpha} (F_{\ell}^{X',\alpha})^* \\ &\quad \times \int df \frac{6H_0^2 \Omega_{\alpha}(f)}{(2\pi)^3 f^3} W_X(f) W_{X'}(f), \end{aligned} \quad (23)$$

where  $X$  and  $X'$  can be  $z$ ,  $E$ , or  $B$ , and the polarization  $\alpha$  can be TE or TB (in general relativity), or more generally ST or SL (scalar modes), or VE or VB (vector modes).<sup>3</sup> Here, the projection factors  $F_{\ell}^{X,\alpha}$  wind up taking relatively simple forms, summarized in Table I. The window functions  $W_X(k)$  are related to the cadence of observations. For the simple assumption that observations are made at two times separated by an interval  $\Delta t$ ,  $W_X(k) = \sin(\pi f \Delta t)$  for all  $X$ . More generally,  $W_E(k) = W_B(k)$ , but  $W_z(k)$  (which comes from different observations) may differ. We make comments about such generalizations in Sec. VI A. In the above equation,  $\Omega_{\alpha}(f)$  is the contribution, per logarithmic frequency interval, of the type- $\alpha$  gravitational wave to the critical density, and  $H_0$  is the Hubble parameter.

The second line of Eq. (23) contributes to the overall amplitude of the correlation function and incorporates all frequency dependencies relating to the gravitational wave

<sup>3</sup>Note that statistical homogeneity requires  $\Omega_{\text{TE}}(f) = \Omega_{\text{TB}}(f)$  and  $\Omega_{\text{VE}}(f) = \Omega_{\text{VB}}(f)$  [38]. The energy densities in the SL and ST modes are, however, not required to be the same.

TABLE I. The projection factors that relate the amplitude of a given TAM wave to its associated observables. These also determine the power spectra, through Eq. (23). The first column  $X$  indicates the gravitational-wave polarization. Here,  $N_\ell = \sqrt{(\ell+2)!/[2(\ell-2)!]}$ .

$X$	$F_\ell^{E,X}$	$F_\ell^{B,X}$	$F_\ell^{z,X}$
ST	$\frac{i}{6}\delta_{\ell 1}$	0	$-\frac{1}{2\sqrt{2}}(\delta_{\ell 0} + \frac{i}{3}\delta_{\ell 1})$
SL	$-\frac{i}{3\sqrt{2}}\delta_{\ell 1} + \frac{i^\ell}{2\sqrt{\ell(\ell+1)}}$	0	$-\frac{i^\ell}{4}\ln(kr_s)$
VE	$\frac{2i}{3\sqrt{2}}\delta_{\ell 1} - \frac{i^\ell}{\sqrt{2\ell(\ell+1)}}$	0	$-\frac{i}{3}\delta_{\ell 1} + \frac{i^\ell}{\sqrt{2\ell(\ell+1)}}$
VB	0	$\frac{i}{3\sqrt{2}}\delta_{\ell 1} - \frac{i^\ell}{\sqrt{2\ell(\ell+1)}}$	0
TE	$-i^\ell \frac{N_\ell^{-1}}{\sqrt{\ell(\ell+1)}}$	0	$\frac{i^\ell}{2}N_\ell^{-1}$
TB	0	$-i^\ell \frac{N_\ell^{-1}}{\sqrt{\ell(\ell+1)}}$	0

and the observation. Omitting this line from Eq. (23), we find the resulting angular correlations functions agree with previous results. We identify our  $C^{\parallel\parallel}(\Theta)$  and  $C^{\perp\perp}(\Theta)$  for the tensor polarizations with  $-\sigma(\Theta)\sin^2\Theta$  and  $\alpha(\Theta)\sin^2\Theta$ , respectively, in Ref. [24]. We also identify our  $C^{\parallel\parallel}(\Theta)$ ,  $C^{\perp\perp}(\Theta)$ , and  $C^{\parallel\perp}(\Theta)$  with  $\Gamma_{x\theta}(\Theta)$ ,  $\Gamma_{y\phi}(\Theta)$ , and  $\Gamma_{z\theta}(\Theta)$ , respectively, for various polarizations in Ref. [26].

#### IV. CALCULATION OF THE POWER SPECTRA AND CORRELATION FUNCTIONS

We now calculate the projection factors  $F_\ell^{X,\alpha}$ , and thus the power spectra.

##### A. The redshift

The redshift  $z$  (the fractional frequency shift relative to the *emitted* frequency) of a photon observed from a pulsar at a distance  $r_s$  in a direction  $\hat{\mathbf{n}}$  in the presence of a spacetime-metric perturbation  $h_{ab}(t, \mathbf{x})$  is [e.g., from Eq. (23.10) in Ref. [39]],

$$z(t, \hat{\mathbf{n}}) = \frac{1}{2} \int_{t-r_s}^t dt' \frac{\partial}{\partial t'} n^a n^b h_{ab}(t', \mathbf{x}(t')), \quad (24)$$

where  $\partial/\partial t'$  acts only on the first argument, and not the time dependence in  $\mathbf{x}(t')$ .

Now consider a perturbation,

$$h_{ab}(\mathbf{x}, t) = 4\pi i^\ell h_{k\ell m}^\alpha \Psi_{(\ell m)ab}^{k,\alpha}(\mathbf{x}) e^{-ikt}, \quad (25)$$

due to a single TAM wave of polarization  $\alpha$  with amplitude  $h_{k\ell m}^\alpha$ . We assume, with the  $e^{-ikt}$  time dependence, that the waves propagate at the speed of light with angular frequency  $\omega = k$ . For the calculation of the redshift, we need the quantity  $n^a n^b \Psi_{(\ell m)ab}^{k,\alpha}(\mathbf{x})$ , which can be written as a spherical harmonic  $Y_{\ell m}(\hat{\mathbf{n}})$  times some radial function

$-R_\ell^{L,\alpha}(kr)$  provided in Appendix A. For example, the radial function for TE is  $R_\ell^{L,TE}(kr) = -N_\ell j_\ell(kr)/(kr)^2$ , where  $N_\ell = \sqrt{(\ell+2)!/[2(\ell-2)!]}$  and  $j_\ell(kr)$  is the spherical Bessel function, and it vanishes for VB and TB. We then find that the redshift  $z$  due to a single  $\alpha$  mode is

$$z(\hat{\mathbf{n}}, t) = -\frac{i}{2} 4\pi i^\ell h_{k\ell m}^\alpha Y_{\ell m}(\hat{\mathbf{n}}) e^{-ikt} \int_0^{kr_s} dx R_\ell^{L,\alpha}(x) e^{ix}, \quad (26)$$

with  $x = kr$ . For example, for TE, this is

$$z(\hat{\mathbf{n}}, t) = \frac{i}{2} 4\pi i^\ell h_{k\ell m}^{TE} N_\ell Y_{\ell m}(\hat{\mathbf{n}}) e^{-ikt} \int_0^{kr_s} dx \frac{j_\ell(x)}{x^2} e^{ix}. \quad (27)$$

We then take the distant-source limit  $kr_s \rightarrow \infty$  and thus infer that

$$z(\hat{\mathbf{n}}, t) = 4\pi i^\ell F_\ell^{z,\alpha} h_{k\ell m}^\alpha Y_{\ell m}(\hat{\mathbf{n}}) e^{-ikt}, \quad (28)$$

with

$$F_\ell^{z,\alpha} = -\frac{i}{2} \int_0^\infty dx R_\ell^{L,\alpha}(x) e^{ix}. \quad (29)$$

For example, for the TE mode, the integral evaluates to

$$F_\ell^{z,TE} = \frac{i^\ell}{2} N_\ell^{-1}. \quad (30)$$

The analogous results for the other five polarizations are provided in Table I.

The pulsar-timing spherical-harmonic coefficient for the observable change in the pulsar frequency, due to mode  $\alpha$ , is then obtained, differencing the result at two different times separated by  $\Delta t$ , by

$$z_{\ell m}(t) = 4\pi i^\ell F_\ell^{z,\alpha} h_{k\ell m}^E (e^{-ik\Delta t} - 1) e^{-ikt}, \quad (31)$$

where here  $t$  is the time of the initial observation. This particular TAM wave then contributes

$$(C_\ell^{zz})_{k\ell m} = (4\pi)^2 |F_\ell^{z,\alpha}|^2 |h_{k\ell m}^E|^2 [2W(k)]^2, \quad (32)$$

to the power spectrum for the redshift observable. Here,  $W(k) \equiv \sin(k\Delta t/2)$  is the frequency-space window function.

Now suppose we have a stochastic background characterized by a power spectrum  $P_h(k)$ , using the conventions/definitions of Sec. V.A in Ref. [31]. We then infer that each spherical-harmonic coefficient  $z_{\ell m}$  takes on a value selected from a distribution with zero mean and variance

$\langle |z_{\ell m}|^2 \rangle = C_\ell^{zz}$ , where the angular power spectrum  $C_\ell^{zz}$  is obtained by summing over all  $\alpha$ -mode TAM waves with the same TAM quantum numbers  $\ell m$ . Thus,

$$C_\ell^{zz,\alpha} = \sum_k (C_\ell^{zz})_{k\ell m} = \frac{4}{\pi} |F_\ell^{z,\alpha}|^2 \int k^2 dk P_h(k) [W(k)]^2. \quad (33)$$

We then use Eq. (A4) to recover the form given in Eq. (23).

### 1. Specific results

*Transverse-traceless modes.* We begin with the transverse-traceless modes that propagate in general relativity. The results in this case are obtained exclusively from the TE modes, since TB does not contribute to the redshift. We obtain from Eq. (33),

$$C_\ell^{zz,\text{GW}} = \frac{12H_0^2 N_\ell^{-2}}{\pi} \int df \frac{\Omega_{\text{GW}}(f)}{f^3} |W_z(f)|^2, \quad (34)$$

where we used  $\Omega_{\text{TE}}(f) = \Omega_{\text{GW}}(f)/2$ , and  $\Omega_{\text{GW}}(f)$  is the gravitational-wave energy density (summing over both polarization states). Since  $C_\ell \propto \ell^{-4}$  at larger  $\ell$ , the power spectrum is very highly peaked at the smallest multipole moments, and particularly the quadrupole. The  $\ell$  dependence of the power spectrum is the same for any functional form of  $\Omega_{\text{GW}}(f)$ , a consequence of the distant-source limit—the observations probe the *local* spacetime-metric perturbation. Using the results of Appendix B, the angular correlation function is found, for the canonical transverse-traceless modes, to be

$$C_\ell^{zz,\text{GW}}(\Theta) = \frac{3H_0^2}{2\pi^2} \int df \frac{\Omega_{\text{GW}}(f)}{f^3} |W_z(f)|^2 \text{HD}(\Theta), \quad (35)$$

where  $\text{HD}(\Theta)$  is the famous Hellings-Downs curve provided in Eq. (B8). The angular correlation function is shown in Fig. 1.

*Vector modes.* The redshift power spectrum for the vector modes is exactly as in Eq. (34), but with  $N_\ell^{-2} \rightarrow [2\ell(\ell+1)]^{-1} - (2/9)\delta_{\ell 1}$ . Simple algebraic manipulation of results in Appendix B yields the vector analog,

$$\begin{aligned} \text{HD}_v(\Theta) &= 2 \sum_{\ell=1}^{\infty} (2\ell+1) \left( \frac{1}{2\ell(\ell+1)} - \frac{2}{9}\delta_{\ell 1} \right) P_\ell(\cos \Theta) \\ &= -2 \ln [\sin(\Theta/2)] - 1 - \frac{4}{3} \cos \Theta, \end{aligned} \quad (36)$$

which is shown in Fig. 1 and agrees with results obtained from real-space calculations [26,28]. The logarithmic divergence as  $\Theta \rightarrow 0$  arises in the harmonic approach given that the summand is  $\sim \ell^{-1}$  at large  $\ell$ . This divergence is regulated by taking  $kr_s$  finite. In practice, the divergence is irrelevant given the finite density of pulsars on the sky.

*Scalar-transverse modes.* The power spectrum is again as in Eq. (34), but now with  $N_\ell^{-2} \rightarrow (\delta_{\ell 0} + \delta_{\ell 1}/9)/8$ . The Hellings-Downs analogue then becomes simply  $1/4 + (1/12)\cos \Theta$ , as shown in Fig. 1 and again in agreement with prior work [28]. In principle, the monopole would be observable if we had a complete handle on timing information from a terrestrial standard clock. In practice, though, errors in timing and timing models can produce monopolar correlations between pulsars [40], rendering the extraction of the monopole difficult. There is also no cross-correlation with angular deflections, since there is no monopole for angular deflections.

*Scalar-longitudinal.* The radial function  $R_\ell^{L,\text{SL}}$  for the SL mode contains a term  $\propto j_\ell(x)$  that renders the radial integral divergent in the distant-source limit  $kr_s \rightarrow \infty$ . This is a consequence of the fact that the light ray from a source aligned with the direction of propagation of a gravitational wave can “surf” the gravitational wave and (unlike the other modes) experiences a stretching in this same direction. The magnitude of the redshift thus accrues monotonically as the light ray propagates from the source. The integral can be performed numerically (or written in terms of hypergeometric functions, which are then determined numerically), but can, using  $j_\ell(x) \sim x^{-1} \cos(x - (\ell+1)\pi/2)$  for  $x \gg \ell$ , be approximated in the  $kr_s \gg 1$  limit by

$$F_\ell^{z,\text{SL}}(k) = -\frac{i^\ell}{4} \ln(kr_s). \quad (37)$$

Note that this result, unlike all the others we encounter in this paper, depends on the wave number  $k$  and on the source distance  $r_s$ . It is also, strictly speaking, valid only for  $kr_s \gg \ell$ . Given the logarithmic dependence on both  $k$  and  $r_s$ , we can obtain rough estimates by fixing the logarithm using some characteristic  $k$  [set, perhaps by the observationally preferred frequency  $f = k/(2\pi) \simeq \text{yr}^{-1}$ ] and source distance (perhaps  $\sim 3$  kpc). With these canonical values  $kr_s \sim 6 \times 10^4$  (justifying the  $kr_s \gg \ell$  assumption), and the logarithm is roughly 10, explaining the roughly order-of-magnitude enhancement inferred numerically in previous work [26,27]. Since the logarithm grows very slowly, the asymptotic expression in Eq. (37) is unlikely to be numerically precise, possibly with significant contributions from subdominant terms.

The multipole-moment ( $\ell$ ) dependence of the power spectrum is also interesting. In the distant-source limit, it is independent of  $\ell$ . Such a power spectrum is that for white noise, which exhibits a correlation function that is nonzero only at zero lag (formally, a Dirac delta function). This may account for numerical evidence for a rapid increase of  $C^{zz}(\Theta)$  as  $\Theta \rightarrow 0$  for the SL mode. Phenomenologically, it implies that the SL mode gives rise to fluctuations that are uncorrelated from one point on the sky to the other. Since the large- $x$  approximation for  $j_\ell(x)$  used to obtain Eq. (37) breaks down for  $\ell \gtrsim kr_s \sim 6 \times 10^4$ , we surmise that the

correlation should be nonzero at angular separations  $\Theta \lesssim 180^\circ/\ell \simeq 10$  arcsec.

We quantify these statements by augmenting the SL projection factor with a Gaussian in  $\ell$ , to  $F_\ell = -(i^\ell/4) \ln(kr_s) e^{-\ell^2/2\ell_{\max}^2}$ , to account for the breakdown in the distant-source limit at  $\ell \gtrsim \ell_{\max}$ . With this, the ‘‘Hellings-Downs’’ curve for the SL modes becomes

$$\begin{aligned} \text{HD}_{\text{SL}}(\Theta) &= \frac{1}{4} \sum_{\ell=0} (2\ell+1) P_\ell(\cos\theta) e^{-\ell^2/2\ell_{\max}^2} \\ &\simeq \frac{\ell_{\max}^2}{4} e^{-\ell_{\max}^2 \theta^2}. \end{aligned} \quad (38)$$

## B. Angular deflections

As derived in prior work [24], the angular deflection of a light ray observed at time  $t$  propagating in the  $\hat{\mathbf{n}}$  direction from a source at distance  $r_s$  is

$$\begin{aligned} (\delta n)^a(\hat{\mathbf{n}}, t) &= \Pi^{ac} n^b \left\{ -\frac{1}{2} h_{bc}(t, \mathbf{0}) + \frac{1}{r_s} \int_0^{r_s} dr [h_{bc}(t-r, r\hat{\mathbf{n}}) \right. \\ &\quad \left. - \frac{r_s-r}{2} n^d \partial_c h_{bd}(t-r, r\hat{\mathbf{n}})] \right\}, \end{aligned} \quad (39)$$

where  $\Pi_{ab}(\hat{\mathbf{n}}) = g_{ab} - \hat{n}_a \hat{n}_b$  projects onto the plane orthogonal to  $\hat{\mathbf{n}}$  (i.e., onto the plane of the sky). Since we are not concerned with sources at cosmological distances, we take the spacetime metric  $g_{ab}$  to be Minkowski. Using the relation [31],

$$\hat{n}^b \hat{n}^d \partial_c h_{bd} = \partial_c (\hat{n}^b \hat{n}^d h_{bd}) - \frac{2}{kr} \Pi_{cb} \hat{n}_d h^{bd}, \quad (40)$$

the angular deflection can be rewritten,

$$\begin{aligned} (\delta n)^a(\hat{\mathbf{n}}, t) &= \Pi^{ac} \left\{ -\frac{1}{2} n^b h_{bc}(t, \mathbf{0}) + \int_0^{r_s} dr \left[ \frac{1}{r} n^b h_{bc}(t-r, r\hat{\mathbf{n}}) \right. \right. \\ &\quad \left. \left. - \frac{r_s-r}{2r_s} \partial_c n^b n^d h_{bd}(t-r, r\hat{\mathbf{n}}) \right] \right\}. \end{aligned} \quad (41)$$

Now consider a single TAM wave of polarization  $\alpha$ , quantum numbers  $k\ell m$ , and amplitude  $h_{k\ell m}^\alpha$ . The first term in Eq. (41), the ‘‘observer’’ term, is obtained by evaluating the coefficients of  $Y_{(\ell m)a}^E(\hat{\mathbf{n}})$  and  $Y_{(\ell m)a}^B(\hat{\mathbf{n}})$  in Eq. (A9) at  $r=0$  (the projection operator  $\Pi^{ac}$  does not affect the E and B vector spherical harmonics, since they are already defined on the 2-sphere of the sky). These turn out to be nonzero only for  $\ell=2$  and only for the ST, SL, VE, and TE coefficients of  $Y_{(\ell m)a}^E(\hat{\mathbf{n}})$ . As a result the first term in Eq. (41) evaluates to  $F_\ell^{E,\alpha(0)} Y_{(\ell m)a}^E(\hat{\mathbf{n}})$ , with  $F_\ell^{E,\alpha(0)} = c\delta_{\ell 2}$  and  $c = -\sqrt{6}/30$  for SL,  $c = \sqrt{3}/30$  for ST, and  $c = (5\sqrt{2})^{-1}$  for VE and TE.

The second term in Eq. (41) (the first term in the integral) receives contributions from all terms in Eq. (A9). The contribution from these terms to the angular deflection is

$$F_\ell^{X,\alpha(1)} = \int_0^{kr_s} \frac{dx}{x} e^{ix} R_\ell^{X,\alpha}(x), \quad (42)$$

where the radial function  $R_\ell^{X,\alpha}(x)$  is the coefficient of the appropriate  $Y_{(\ell m)a}^X(\hat{\mathbf{n}})$  in Eq. (A9), and  $X = \{E, B\}$ . The integrals are all finite and easily evaluated in the distant-source limit  $kr_s \rightarrow \infty$ .

The last term in Eq. (41) receives, as discussed at the end of Appendix A, contributions only from the  $Y_{(\ell m)a}^L(\hat{\mathbf{n}})$  terms in Eq. (A9). The evaluation of this term is then aided by the relation  $\Pi_{ab} \nabla^b Y_{(\ell m)}(\hat{\mathbf{n}}) = -M_{\perp a} Y_{(\ell m)}(\hat{\mathbf{n}})/r = -\sqrt{\ell(\ell+1)} Y_{(\ell m)a}^E(\hat{\mathbf{n}})/r$ , where  $M_{\perp a}$  is the gradient operator on the sphere [31]. The contributions from these terms to the angular deflection are

$$F_\ell^{E,\alpha(2)} = -\frac{\sqrt{\ell(\ell+1)}}{2} \int_0^{kr_s} \frac{dx}{x} e^{ix} \frac{kr_s-x}{kr_s} R_\ell^{L,\alpha}(x). \quad (43)$$

The integrals are again all finite and easily evaluated in the distant-source limit  $kr_s \rightarrow \infty$ .

Putting the results together, the angular deflection from this TAM mode is

$$(\delta n)_a(\hat{\mathbf{n}}) = 4\pi i^\ell h_{k\ell m}^\alpha e^{-ikt} [F_\ell^{E,\alpha} Y_{(\ell m)a}^E(\hat{\mathbf{n}}) + F_\ell^{B,\alpha} Y_{(\ell m)a}^B(\hat{\mathbf{n}})], \quad (44)$$

where the  $F_\ell^{E,\alpha}$  and  $F_\ell^{B,\alpha}$  are the sums of the three individual contributions and listed in Table I. Interestingly, the observer terms for  $F_\ell^{E,\alpha}$  augment the radial-integral contributions that arise for  $\ell=2$ , yielding very compact expressions in the table. The corresponding power spectra, as given in Eq. (23), are then obtained, following the same steps as above for the redshift, by taking the difference between the angular deflections evaluated at two different times separated by  $\Delta t$ , and then squaring and then summing over all wave numbers  $k$  for a given  $\ell m$ .

## 1. Specific results

*Transverse-traceless modes.* The power spectra for the gravitational waves that appear in general relativity are

$$\begin{aligned} C_\ell^{EE,\text{GW}} &= C_\ell^{BB,\text{GW}} \\ &= \frac{12H_0^2 N_\ell^{-2}}{\pi \ell(\ell+1)} \int df \frac{\Omega_{\text{GW}}(f)}{f^3} |W_z(f)|^2, \end{aligned} \quad (45)$$

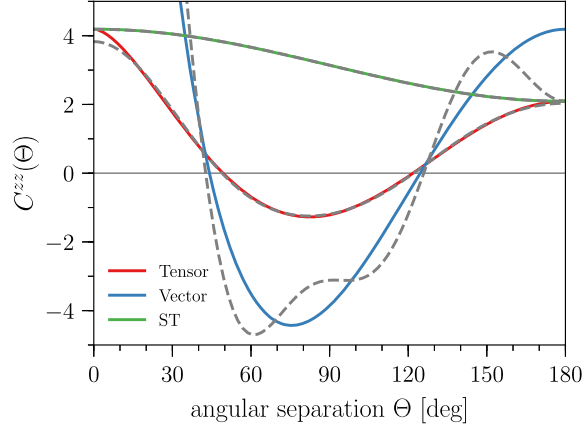


FIG. 1. The  $C^{zz}(\Theta)$  correlation functions for the transverse-traceless tensor modes, vector modes, and the ST mode. They are normalized by omitting second line in Eq. (23). The solid curves show the exact results in the distant-source limit, and dashed curves show the results from truncating the multipole expansion at  $\ell_{\max} = 5$ .

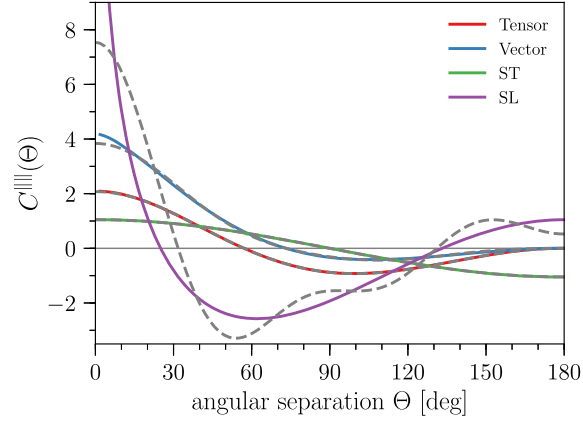


FIG. 2. The  $C^{|||}(\Theta)$  correlation functions for the transverse-traceless tensor modes, vector modes, and the ST and SL modes. They are normalized by omitting second line in Eq. (23). The solid curves show the exact results in the distant-source limit, and dashed curves show the results from truncating the multipole expansion at  $\ell_{\max} = 5$ .

and we note that this is equal to  $[\ell(\ell + 1)]^{-1} C_{\ell}^{zz, \text{GW}}$ . As a result, the correlation functions  $\beta^{EE}(\Theta) = \beta^{BB}(\Theta) \propto \text{HD}(\Theta)$ , as noted previously.<sup>4</sup> The  $|||$  and  $\perp\perp$  correlation functions are easily evaluated numerically and shown in Fig. 2. Although they are nominally obtained from an infinite sum, numerically precise results can be obtained from just the first few terms, given the steep drop of  $C_{\ell}$  with  $\ell$ , as seen in Figs. 2 and 3. We have checked numerically that these correlation functions agree with those in prior work.

<sup>4</sup>An explanation of this coincidence is provided in Appendix C.

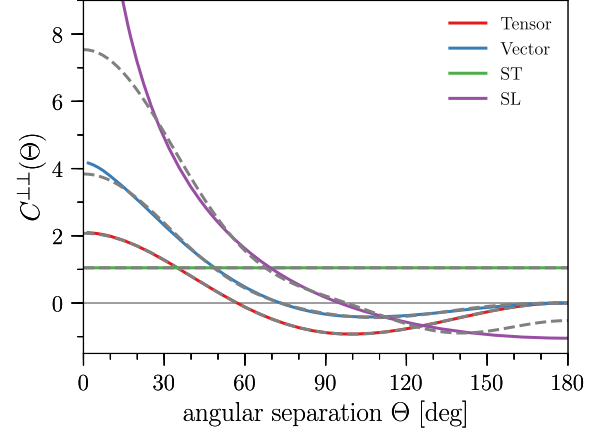


FIG. 3. The same as Fig. 2, but for the  $C^{\perp\perp}(\Theta)$  correlation functions. The correlation functions are the same as  $C^{|||}(\Theta)$  for the vector and tensor modes.

They can also be shown analytically to agree by writing the associated Legendre polynomials  $P_{\ell}^2(x)$  and  $P_{\ell}^1(x)$  in the definitions of  $G_{(\ell 1)}(x)$  and  $G_{(\ell 2)}(x)$  in terms of Legendre polynomials and then using the techniques of Appendix B. The derivation is straightforward but not particularly illuminating, and so we leave out the details.

*Vector modes.* The EE/BB power spectra for these modes are again equal and turn out to be  $C_{\ell}^{EE, \text{vector}} = C_{\ell}^{BB, \text{vector}} \propto [\ell(\ell + 1)]^{-2}$  for  $\ell > 1$ , with an additional contribution (that is the same for EE and BB) for  $\ell = 1$ . The E/B correlation functions  $\beta^{EE}(\Theta) = \beta^{BB}(\Theta) = \text{HD}_v(\Theta)$  in this case turn out to be the same as the angular redshift correlation (which can again be understood simply from the arguments in Appendix C). Again, the rotationally invariant angular correlation functions are shown in Figs. 2 and 3 and agree with those in Refs. [26,27].

*Scalar modes.* Statistical homogeneity implies equal TE and TB powers for transverse-traceless modes and equal VE and VB powers for vector modes. There is, however, no corresponding symmetry requirement that the SL and ST modes should have the same power [20,41]. The relative amplitudes may depend on the details of the alternative-gravity theory.<sup>5</sup> For example, Brans-Dicke theory has a massless scalar that excites the ST mode [42]. In  $f(R) = R + \alpha R^2$  gravity, there is a single massive scalar mode that introduces a mixture of SL and ST modes, with a ratio dependent on  $\alpha$  [43]. In the more general case of Horndeski gravity, the trend is the same: a massless scalar mode excites ST modes, while a massive scalar excites both SL and ST modes [44]. The two modes must therefore be considered separately.

<sup>5</sup>We reiterate that the calculations in this work assume gravitational waves propagate at the speed of light; if this is not the case, the modified dispersion relation  $\omega(k)$  must be used in the expression for plane-wave propagation  $e^{-i\omega(k)t}$ .

The EE correlation function  $\beta^{EE}(\Theta)$  for the SL mode exhibits a Dirac delta function with an added dipole, and for the ST mode it is a pure dipole. The B-mode correlation  $\beta^{BB}(\Theta) = 0$  for both scalar modes. The rotationally invariant angular correlation functions are shown in Figs. 2 and 3; note that  $C^{\parallel\parallel}(\Theta)$  and  $C^{\perp\perp}(\Theta)$  are unequal for these modes. The angular correlations for the ST modes are simply  $C^{\parallel\parallel} = (3/8\pi)C_{\ell=1}^{EE} \cos \Theta$  and  $C^{\perp\perp} = (3/8\pi)C_{\ell=1}^{EE}$ .

## V. REDSHIFT-DEFLECTION CROSS-CORRELATION

Since the redshift and E-mode deflection angle both arise from the same TE TAM waves, there is a cross-correlation between these two observables characterized by a power spectrum,

$$C_{\ell}^{zE} = \langle z_{\ell m} E_{\ell m}^* \rangle. \quad (46)$$

Moreover, since the  $k$  integrands in the expressions for the E-mode and redshift power spectra are identical, this cross-correlation is *exact* (for concurrent PTA/astrometry observations) in the distant-source limit; i.e.,

$$C_{\ell}^{zE} = \sqrt{C_{\ell}^{EE} C_{\ell}^{zz}}, \quad (47)$$

(except for the SL mode, for which the redshift is sensitive to the location of the source, while the deflection is dominated by the local metric perturbations, resulting in essentially no cross-correlation). As a result, pulsar-timing and astrometry probes of the stochastic gravitational-wave background can be used to cross-check. This exact cross-correlation moreover suggests that astrometry and

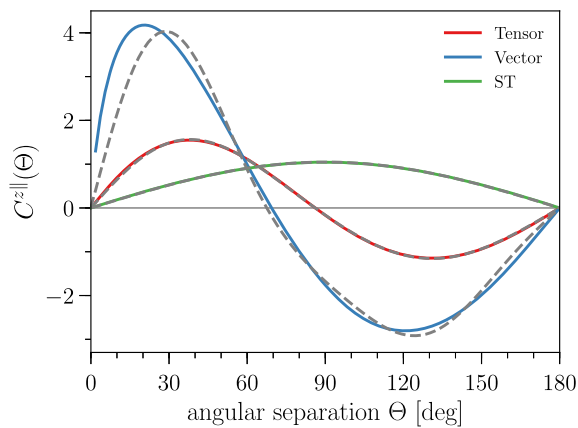


FIG. 4. The  $C^{\parallel\parallel}(\Theta)$  correlation functions for the transverse-traceless tensor modes, vector modes, and the ST mode. They are normalized by omitting second line in Eq. (23). The solid curves show the exact results in the distant-source limit, and dashed curves show the results from truncating the multipole expansion at  $\ell_{\max} = 5$ .

pulsar-timing surveys can be used to complement each other to optimize sky coverage in the event that there are blind regions in the sky in one survey or the other.

These cross-correlations can be obtained numerically and are provided in Fig. 4. Again, the correlations are well characterized by the lowest multipole moments. The analytic results for  $C^{\parallel\parallel}(\Theta)$  in Eqs. (53) and (55) of Ref. [26], for tensor and vector modes, respectively, can be obtained from the relation,

$$P_{\ell}^1(\cos \Theta) = \frac{\ell(\ell+1)P_{\ell+1}(\cos \Theta) - P_{\ell-1}(\cos \Theta)}{2\ell+1 \sin \Theta}, \quad (48)$$

and those in Appendix B.

## VI. GRAVITATIONAL-WAVE WINDOW FUNCTIONS, POINTING, AND CHIRALITY

### A. Time evolution and window functions

We now note that all of the predicted power spectra can be written as the product of a function of multipole moment  $\ell$  and an integral,

$$\int k^2 dk P_h(k) [W(k; \Delta t)]^2, \quad (49)$$

for the power spectrum (with analogous results for vector and scalar modes). The absence of any dependence of the angular structure on the form of  $P_h(k)$  arises because the observables arise only in the distant-source limit. We probe with these measurements only the *local* spacetime-metric perturbation; there are no long-range spatial correlations imprinted on the observed angular correlations.

We now focus on the window function  $W(k; \Delta t) = \sin(k\Delta t/2)$  obtained by assuming redshifts and stellar positions were obtained at two instantaneous times separated by an interval  $\Delta t$ . The window function is then just the Fourier transform of a time “exposure,”  $\delta_D(t + \Delta t) - \delta_D(t)$ . More realistically, the measurements may be done over some range of times, or (for pulsar timing) inferred from timing residuals. The detailed functional form of the window function  $W(k)$  will therefore differ from the simple  $W(k; \Delta t)$  inferred here. Regardless, we expect  $[W(k)]^2 \propto (k\Delta t)^2$  for  $k\Delta t \ll 1$ , where  $\Delta t \sim \text{yrs}$  is the overall time interval in which measurements are done. Also, there will be a suppression at high  $k$  that arises from the finite duration of any particular measurement made.

As discussed in Sec. V above, the angular cross-correlation between the astrometry and pulsar-timing signals are *exact* if the two observing periods coincide. More generally, though, the observations will not necessarily be concurrent, and so the astrometry-PTA cross-correlation will be degraded. For example, suppose the pulsar-timing measurements are done at two times  $t$  and  $t + \Delta t$ , while the astrometry measurements are done at times  $t + \delta t$  and  $t + \delta t + \Delta t$ . The cross-correlation coefficient will then be

$$\begin{aligned}
r &\equiv \frac{\langle z_{\ell m} E_{\ell m}^* \rangle}{\sqrt{\langle |z_{\ell m}|^2 \rangle \langle |E_{\ell m}|^2 \rangle}} \\
&= \frac{\int \frac{dk}{2\pi} P(k) \sin^2(k\Delta t/2) \cos(k\delta t/2)}{\int \frac{dk}{2\pi} P(k) \sin^2(k\Delta t/2)}. \quad (50)
\end{aligned}$$

One can see that if the PTA and astrometry measurements are separated by times  $\delta t \lesssim \Delta t$ , the cross-correlation remains strong and then becomes weak for  $\delta t \gtrsim \Delta t$ .

Here we have assumed that pulsar-timing and astrometry results are each made at only two epochs. In this case, the measured spherical-harmonic coefficients for each  $\ell m$  receive contributions from an array of TAM waves  $h_{k\ell m}$  for an array of values of wave number  $k$ , and if the observations are concurrent, the *same* set of TAM waves. If, however, measurements are made over a larger set of times—say  $N$  times, rather than two—then the measurements can be decomposed into power spectra for  $N - 1$  different window functions, which probe different ranges of frequencies. If so, then information about the distribution of the wave numbers  $k$  that give rise to the signal, for each  $\ell m$ , can be extracted. In other words, with time measurements, the three-dimensional spacetime-metric perturbation (and not just some two-dimensional projection) can begin to be reconstructed. We leave an elaboration of this frequency-space analysis for future work.

Suppose now that the stochastic background has an energy density  $\Omega_{\text{gw}}(f) \sim \text{constant}$ , which is expected for the nearly scale-invariant spectrum ( $n_t \simeq 0$ ) generated from inflation. In this case, the window-function behavior  $W(k) \propto k$  for  $k\Delta t \ll 1$  results in an equal contribution per logarithmic frequency interval (at frequencies  $k\Delta t \ll 1$ ) to the observables. If so, then the distant-source limit we have employed is not strictly speaking valid. We have checked (but leave details for elsewhere), that the contribution of longer-wavelength modes (i.e., those with  $kr_s \lesssim 1$ ) to  $\ell \geq 3$  multipole moments is suppressed relative to what is inferred using the distant-source limit. The contribution to the quadrupole is, however, a bit larger. Still, given that the amplitude of the inflationary background is expected to be far too small ( $\Omega_{\text{gw}} h^2 \sim 10^{-16}$  at frequencies  $f \sim 10^{-9}$  Hz) to be accessed with PTAs and astrometry [45], we consider this point academic.

The background more realistically accessible is that from the merger of supermassive black holes. If the SMBH binaries are all circular, then the expected background has  $\Omega_{\text{gw}} \propto f^{2/3}$ , in which case the contributions of longer-wavelength gravitational waves to the observables are suppressed. The suppression is even stronger if the SMBH orbits are eccentric (e.g., the scaling may be as strong as  $\Omega_{\text{gw}} \propto f^3$ ) [15,46–48]. We thus conclude that the distant-source limit is valid for the SMBH signal.

## B. Chirality

Here we have taken the normal modes of the transverse-traceless tensor field to be  $\Psi_{(\ell m)ab}^{k,\text{TE}}$  and  $\Psi_{(\ell m)ab}^{k,\text{TB}}$ . Statistical homogeneity then requires that these have equal power [38].

However, we could have equally well worked alternatively with a helicity basis, in terms of TAM modes  $\Psi_{(\ell m)ab}^{k,\pm} = 2^{-1/2}[\Psi_{(\ell m)ab}^{k,\text{TE}} \pm i\Psi_{(\ell m)ab}^{k,\text{TB}}]$ . These two modes represent right- and left-circularly polarized gravitational waves. If parity is unbroken, then the energy densities in the two circular-polarization states should be the same. If so, the cross-correlations  $C_{\ell}^{zB} = C_{\ell}^{EB} = 0$ .

However, it is conceivable, and perhaps even to be expected, that the stochastic background observed by pulsar timing and astrometry may be chiral—i.e., may exhibit a preponderance of one handedness over the other. The emission from SMBH binaries is expected to be circularly polarized, to some degree (depending on the orientation of the binary relative to the line of sight). If the background is dominated by a small number  $N$  of SMBHs (see, e.g., Refs. [15,49–51]), then the fractional difference between the powers in the two helicities should be  $\sim N^{-1/2}$ ; i.e., not too small. It is thus not advisable to assume that these cross-correlations will be zero and can thus be used to as null tests for systematics. On the other hand, these parity-breaking power spectra  $C_{\ell}^{zB}$  and  $C_{\ell}^{EB}$  (or equivalently, the parity-breaking  $z_{\perp}$  and  $\parallel_{\perp}$  correlation functions) should be pursued observationally along with the others, as they may shed light on the nature of the sources that give rise to the background. Chirality probes that can be constructed from time-sequence information [52] should also be similarly employed. We moreover note that these cross-correlations provide pulsar timing and astrometry with a capability to test the chirality of the gravitational-wave background in a frequency regime previously thought to be inaccessible [53].

## VII. CONCLUSIONS

Here we have employed a total-angular-momentum formalism to describe the angular correlations in pulsar-timing and astrometry probes of a stochastic gravitational-wave background. Results were presented both in terms of angular power spectra and in terms of angular correlation functions and for all six polarizations that may arise in alternative-gravity theories. Redshift-astrometry cross-correlations were provided for the first time for all six polarizations. An Appendix describes an alternative way to rederive simply the power-spectrum results from plane waves. The dependence of the astrometry signal on the frequency spectrum of the gravitational-wave background was clarified, and it was speculated that information on the local three-dimensional metric perturbation might be inferred by the inclusion of time-sequence information. We also emphasized that the parity-breaking cross-correlations, usually assumed to be zero, will not

necessarily vanish for stochastic backgrounds generated by supermassive-black-hole binaries.

A natural next step would be to ask whether a detected gravitational-wave background exhibits any preferred direction. One possible way to search for such asymmetries is with bipolar spherical harmonics [54–56], which could be used to seek, for example, a dipole asymmetry in the strength of the gravitational-wave signal. It may also be worthwhile to consider merging the techniques presented here with other novel approaches, such as those involving gravitational-wave Stokes parameters [57]. Elaboration of the details and development of such strategies is left for future work.

We hope that the mathematical tools and calculational results we have presented will be of value in further characterization and exploration of stochastic backgrounds.

## ACKNOWLEDGMENTS

We thank E. Berti for useful discussions. This work was supported at Johns Hopkins in part by NASA Grant No. NNX17AK38G, NSF Grant No. 0244990, and the Simons Foundation. L.D. is supported at the Institute for Advanced Study by NASA through Einstein Postdoctoral Fellowship Grant No. PF5-160135 awarded by the Chandra X-ray Center, which is operated by the Smithsonian Astrophysical Observatory for NASA under Contract No. NAS8-03060.

## APPENDIX A: REVIEW OF TOTAL-ANGULAR-MOMENTUM WAVES

### 1. The standard decomposition

The most general symmetric tensor field  $h_{ab}(\mathbf{x}) = h_{(ab)}(\mathbf{x}) \equiv [h_{ab}(\mathbf{x}) + h_{ba}(\mathbf{x})]/2$  can be decomposed into a trace component  $h(\mathbf{x})$ , a longitudinal component  $\xi(\mathbf{x})$ , two vector components  $w_a$  (with  $\nabla^a w_a = 0$ ), and two transverse-traceless tensor components  $h_{ab}^{\text{TT}}$  (which satisfy  $\nabla^a h_{ab}^{\text{TT}} = 0$  and  $h^a_a = 0$ ), as

$$h_{ab} = hg_{ab} + \left( \nabla_a \nabla_b - \frac{1}{3} g_{ab} \nabla^2 \right) \xi + \nabla_{(a} w_{b)} + h_{ab}^{\text{TT}}. \quad (\text{A1})$$

The most general rank-two symmetric  $3 \times 3$  tensor can be expanded as

$$h_{ab}(\mathbf{x}) = \sum_{k,s} \epsilon_{ab}^s(\hat{k}) h_s(\mathbf{k}) e^{ik \cdot \mathbf{x}} + cc, \quad (\text{A2})$$

in terms of Fourier modes of wave vector  $\mathbf{k}$  and in terms of six polarization states  $\epsilon_{ab}^s(\hat{k})$ , where  $s = \{0, z, x, y, +, \times\}$ , for the trace, longitudinal, two vector, and two transverse-traceless polarizations, respectively, with amplitudes  $h_s(\mathbf{k})$  [58]. The quantity  $cc$  denotes the complex conjugate of the first term. The polarization tensors are normalized such that  $\epsilon^{sab} \epsilon_{ab}^{s'} = 2\delta_{ss'}$ . The two transverse-traceless polarization

states that propagate in general relativity have  $k^a \epsilon_{ab}^{+, \times} = 0$ . Power spectra  $P_h(k)$  for these transverse-traceless gravitational waves are defined by

$$\langle h_s(\mathbf{k}) h_{s'}(\mathbf{k}') \rangle = \delta_{ss'} (2\pi)^3 \delta_D(\mathbf{k} - \mathbf{k}') \frac{P_h(k)}{4}, \quad (\text{A3})$$

for  $s, s' = \{+, \times\}$ .

To connect with prior work on pulsar timing and astrometry, we note that with these conventions, the wave number  $k = 2\pi f$  in terms of the gravitational-wave frequency  $f$ , and

$$P_h(2\pi f) = \frac{3H_0^2 \Omega_{\text{gw}}(f)}{8\pi^3 f^5} = \frac{1}{2\pi f^2} S_h(f) = \frac{1}{4\pi f^3} h_c^2(f), \quad (\text{A4})$$

in terms of the contribution  $\Omega_{\text{gw}}(f)$  per unit logarithmic frequency interval to the critical density (and  $H_0$  is the Hubble parameter), the gravitational-wave spectral density  $S_h(f)$  [16], and  $h_c(f)$ , the dimensionless amplitude per logarithmic frequency interval. To be precise, the total gravitational-wave energy density, summing over all frequencies, is  $\rho_{\text{gw}} = \rho_c \int (df/f) \Omega_{\text{gw}}(f)$ , where  $\rho_c = 3H_0^2/(8\pi G)$  is the critical density.

### 2. Total-angular-momentum waves

TAM waves [31] provide an alternative complete orthonormal set of basis functions for tensor fields. Here, the Fourier wave vector  $\mathbf{k}$  is replaced by quantum numbers  $k\ell m$ , where  $k$  is a wave number and  $\ell m$  are TAM quantum numbers. The 5 trace-free polarizations are replaced by 5 sets of TAM modes, which include L (a trace-free longitudinal mode), VE and VB (two vector modes), and TE and TB (the two transverse-traceless modes). We augment the formalism of Ref. [31] to include a trace degree of freedom. To facilitate comparison with prior astrometry work, we also construct from the L mode tensor harmonic and the scalar harmonic a ST mode and a SL mode to accord with those of Refs. [26–28].

Then, any symmetric  $h_{ab}(\mathbf{x})$  can be expanded,

$$h_{ab}(\mathbf{x}) = \sum_{ak\ell m} 4\pi i^\ell h_{k\ell m}^\alpha \Psi_{(\ell m)ab}^{k,\alpha}(\mathbf{x}) + cc, \quad (\text{A5})$$

in terms of TAM waves  $\Psi_{(\ell m)ab}^{k,\alpha}(\mathbf{x})$ . Here,  $\sum_k$  is a shorthand for  $\int k^2 dk / (2\pi)^3$ , and  $\alpha$  is summed over ST, SL, VE, VB, TE, and TB. The VE/VB/TE/TB TAM waves are as given in Ref. [31].

The SL and ST modes are

$$\Psi_{(\ell m)ab}^{\text{ST}}(\mathbf{x}) = \frac{\sqrt{2}}{3} \Psi_{(\ell m)}(\mathbf{x}) g_{ab} + \sqrt{\frac{1}{3}} \Psi_{(\ell m)ab}^{\text{L}}(\mathbf{x}), \quad (\text{A6})$$

$$\Psi_{(\ell m)ab}^{\text{SL}}(\mathbf{x}) = \frac{1}{3}\Psi_{(\ell m)}(\mathbf{x})g_{ab} - \sqrt{\frac{2}{3}}\Psi_{(\ell m)ab}^{\text{L}}(\mathbf{x}), \quad (\text{A7})$$

where  $\Psi_{(\ell m)}(\mathbf{x}) = j_\ell(kr)Y_{\ell m}(\hat{\mathbf{n}})$  is the scalar TAM wave and  $j_\ell(kr)$  is the spherical Bessel function. The ST TAM wave  $\Psi_{(\ell m)ab}^{\text{ST}}(\mathbf{x})$  has components only transverse to the direction of its gradients, and  $\Psi_{(\ell m)ab}^{\text{SL}}(\mathbf{x})$  is entirely aligned with the gradient. These TAM waves are normalized in accord with the conventions of Ref. [31].

If the metric perturbation is constructed of wavelike solutions that propagate at the speed of light, then the time-dependent metric perturbation  $h_{ab}(\mathbf{x}, t)$  is obtained by multiplying the summand in Eq. (A5) by  $e^{-ikt}$ . If we are dealing with a stochastic background of general-relativistic gravitational waves, then the sum is only over TE/TB modes. In a statistically isotropic stochastic background of GR gravitational waves, the TAM-wave coefficients are statistically independent and taken from a random distribution with variance  $P_h(k)$ ; i.e.,

$$\langle (h_{k\ell m}^\alpha)^* h_{k'\ell' m'}^\beta \rangle = \frac{(2\pi)^3}{2k^2} P_h(k) \delta_{\ell\ell'} \delta_{mm'} \delta_{\alpha\beta} \delta(k-k') \quad (\text{A8})$$

for the TE/TB modes. In alternative-gravity theories, there will be analogous expressions for VE/VB, SL, and ST modes in terms of vector and scalar power spectra, if such modes exist and propagate. Note that the TE/TB modes exist only for  $\ell \geq 2$  and the VE/VB modes for  $\ell \geq 1$ . Note also that statistical homogeneity requires that  $P_{\text{TE}}(k) = P_{\text{TB}}(k)$  and  $P_{\text{VE}}(k) = P_{\text{VB}}(k)$  [38], but the power spectra for SL and ST may most generally differ.

Reference [31] provides an array of results on the properties of these TAM waves, related scalar and vector TAM waves, and several alternative TAM-wave bases. In particular, Eq. (94) in that paper provides the projections of these TAM waves onto an orthonormal basis determined by unit vectors in the radial ( $\hat{\mathbf{n}}$ ) and angular ( $\hat{\boldsymbol{\theta}}$ , and  $\hat{\boldsymbol{\phi}}$ ) directions in the usual spherical coordinates. The central quantities we will need for this work are  $n^b \Psi_{(\ell m)ab}^{\alpha,k}(\mathbf{x})$ . From Eq. (94) of Ref. [31], and our definition of the SL and ST modes, we have

$$\begin{aligned} \hat{n}^a \Psi_{(\ell m)ab}^{\text{SL}}(\mathbf{x}) &= \sqrt{\ell(\ell+1)} \frac{1}{kr} \left( j'_\ell(kr) - \frac{j_\ell(kr)}{kr} \right) Y_{(\ell m)b}^E(\hat{\mathbf{n}}) - \left[ 2 \frac{j'_\ell(kr)}{kr} + \left( 1 - \frac{\ell(\ell+1)}{(kr)^2} \right) j_\ell(kr) \right] Y_{(\ell m)b}^L(\hat{\mathbf{n}}), \\ \hat{n}^a \Psi_{(\ell m)ab}^{\text{ST}}(\mathbf{x}) &= -\frac{1}{\sqrt{2}} \left[ \sqrt{\ell(\ell+1)} \frac{1}{kr} \left( j'_\ell(kr) - \frac{j_\ell(kr)}{kr} \right) Y_{(\ell m)b}^E(\hat{\mathbf{n}}) - \left( 2 \frac{j'_\ell(kr)}{kr} - \frac{\ell(\ell+1)}{(kr)^2} j_\ell(kr) \right) Y_{(\ell m)b}^L(\hat{\mathbf{n}}) \right], \\ \hat{n}^a \Psi_{(\ell m)ab}^{\text{VE}}(\mathbf{x}) &= \sqrt{2} \left[ \frac{j'_\ell(kr)}{kr} + \left( \frac{1}{2} + \frac{(1-\ell-\ell^2)}{(kr)^2} \right) j_\ell(kr) \right] Y_{(\ell m)b}^E(\hat{\mathbf{n}}) - \frac{\sqrt{2\ell(\ell+1)}}{kr} \left( j'_\ell(kr) - \frac{j_\ell(kr)}{kr} \right) Y_{(\ell m)b}^L(\hat{\mathbf{n}}), \\ \hat{n}^a \Psi_{(\ell m)ab}^{\text{VB}}(\mathbf{x}) &= -\frac{i}{\sqrt{2}} \left( j'_\ell(kr) - \frac{j_\ell(kr)}{kr} \right) Y_{(\ell m)b}^B(\hat{\mathbf{n}}), \\ \hat{n}^a \Psi_{(\ell m)ab}^{\text{TE}}(\mathbf{x}) &= -N_\ell \frac{j_\ell(kr)}{(kr)^2} Y_{(\ell m)b}^L(\hat{\mathbf{n}}) - \frac{N_\ell}{\sqrt{\ell(\ell+1)}} \left( \frac{j'_\ell(kr)}{kr} + \frac{j_\ell(kr)}{(kr)^2} \right) Y_{(\ell m)b}^E(\hat{\mathbf{n}}), \\ \hat{n}^a \Psi_{(\ell m)ab}^{\text{TB}}(\mathbf{x}) &= -i \frac{N_\ell}{\sqrt{\ell(\ell+1)}} \frac{j_\ell(kr)}{kr} Y_{(\ell m)b}^B(\hat{\mathbf{n}}), \end{aligned} \quad (\text{A9})$$

with  $N_\ell = \sqrt{(\ell+2)!/[2(\ell-2)!]}$ . Note that these vectorial quantities have a projection onto a vector spherical harmonic  $Y_{(\ell m)a}^L(\hat{\mathbf{n}}) \equiv -n_a Y_{\ell m}(\hat{\mathbf{n}})$ , which points along the radial direction, and another onto either the vector spherical harmonic  $Y_{(\ell m)a}^E(\hat{\mathbf{n}})$  or  $Y_{(\ell m)a}^B(\hat{\mathbf{n}})$ , which lie in the plane of the sky. We thus define radial functions  $R_\ell^{L,\alpha}(x)$  and  $R_\ell^{E,\alpha}(x)$  through

$$\hat{n}^a \Psi_{(\ell m)ab}^\alpha(\mathbf{x}) = R_\ell^{L,\alpha}(kr) Y_{(\ell m)b}^L(\hat{\mathbf{n}}) + R_\ell^{E,\alpha}(kr) Y_{(\ell m)a}^E(\hat{\mathbf{n}}), \quad (\text{A10})$$

and analogously for  $R_\ell^{B,\alpha}(x)$ .

We will also need in our calculations the quantities  $n^a n^b \Psi_{(\ell m)ab}^{\alpha,k}(\mathbf{x})$ , which are obtained from the above expressions by replacing  $Y_{(\ell m)a}^L(\hat{\mathbf{n}})$  by  $-Y_{\ell m}(\hat{\mathbf{n}})$  and ignoring the E/B components, given the orthogonality of the E/B vector spherical harmonics to the radial direction  $\hat{\mathbf{n}}$ .

## APPENDIX B: USEFUL LEGENDRE-POLYNOMIAL RELATIONS

Here we show how to derive the Hellings-Downs curve from a power spectrum  $C_\ell \propto (\ell-2)!/(\ell+2)!$  for  $\ell \geq 2$  and from the fact that  $\text{HD}(\Theta) = \sum_\ell (2\ell+1) C_\ell P_\ell(\cos \Theta)$ . Expanding this quantity using partial fractions yields

$$\text{HD}(\Theta) = \sum_{\ell=2}^{\infty} (2\ell+1) \frac{(\ell-2)!}{(\ell+2)!} P_{\ell}(\cos \Theta) = \frac{1}{2} \sum_{\ell=2}^{\infty} \left( \frac{1}{\ell-1} - \frac{1}{\ell} - \frac{1}{\ell+1} + \frac{1}{\ell+2} \right) P_{\ell}(\cos \Theta). \quad (\text{B1})$$

Each of these four infinite sums can be calculated using the generating function of the Legendre polynomials, which is given by

$$\frac{1}{\sqrt{t^2 - 2tx + 1}} = \sum_{n=0}^{\infty} t^n P_n(x). \quad (\text{B2})$$

For example, let us rewrite the first partial fraction as

$$\frac{1}{\ell-1} = \int_0^{\infty} e^{-z(\ell-1)} dz. \quad (\text{B3})$$

Then we can rewrite the sum as

$$\begin{aligned} \sum_{\ell=2}^{\infty} \frac{1}{\ell-1} P_{\ell}(\cos \Theta) &= \int_0^{\infty} e^z \sum_{\ell=2}^{\infty} e^{-z\ell} P_{\ell}(\cos \Theta) dz = \int_0^{\infty} e^z \left( \frac{1}{\sqrt{e^{-2z} - 2xe^{-z} + 1}} - 1 - e^{-zx} \right) dz \\ &= \int_1^{\infty} \left( \frac{y}{\sqrt{1-2xy+y^2}} - 1 - \frac{x}{y} \right) dy = 1 - x - \sqrt{2-2x} + x \ln \left( \frac{2}{1-x+\sqrt{2-2x}} \right), \end{aligned} \quad (\text{B4})$$

where  $x = \cos \Theta$ . Similar calculations for the other sums give

$$\sum_{\ell=2}^{\infty} \frac{1}{\ell} P_{\ell}(\cos \Theta) = -x + \ln \left( \frac{2}{1-x+\sqrt{2-2x}} \right) \quad (\text{B5})$$

$$\sum_{\ell=2}^{\infty} \frac{1}{\ell+1} P_{\ell}(\cos \Theta) = -1 - \frac{1}{2}x + \ln \left( 1 + \sqrt{\frac{2}{1-x}} \right) \quad (\text{B6})$$

$$\sum_{\ell=2}^{\infty} \frac{1}{\ell+2} P_{\ell}(\cos \Theta) = -\frac{3}{2} - \frac{1}{3}x + \sqrt{2-2x} + x \ln \left( 1 + \sqrt{\frac{2}{1-x}} \right). \quad (\text{B7})$$

We then obtain the Hellings-Downs angular correlation function,

$$\text{HD}(\Theta) = \frac{1}{4} + \frac{1}{12}x + \frac{1}{2} \ln \left( \frac{1-x}{2} \right) - \frac{x}{2} \ln \left( \frac{1-x}{2} \right) = \frac{1}{2}(1-x) \log \left[ \frac{1}{2}(1-x) \right] - \frac{1}{6} \left[ \frac{1}{2}(1-x) \right] + \frac{1}{3}. \quad (\text{B8})$$

### APPENDIX C: ALTERNATIVE DERIVATION OF POWER SPECTRA

Here we present an alternative derivation of the redshift and angular-deflection power spectra (see also Ref. [59]). The calculation begins with the well-known angular dependence,<sup>6</sup>

$$z(\hat{\mathbf{n}}) = \frac{n^a n^b h_{ab}}{2(1 + \hat{\mathbf{p}} \cdot \hat{\mathbf{n}})} \quad (\text{C1})$$

of the redshift in the presence of a gravitational wave traveling in the  $\hat{\mathbf{p}}$  direction. For example, for a transverse-traceless gravitational wave in the  $\hat{\mathbf{z}}$  direction with + polarization, this becomes

$$z(\hat{\mathbf{n}}) \propto (1 - \cos \theta) \cos 2\phi. \quad (\text{C2})$$

<sup>6</sup>Note that this function has an unphysical discontinuity at  $\cos \theta \rightarrow -1$ . This is smoothed by the source term. It can be shown that the neglect of the source term has no effect on the subsequent derivation, though.

The spherical-harmonic coefficients for this angular pattern are

$$z_{\ell m} = \int d\hat{n} Y_{\ell m}(\hat{n}) z(\hat{n})$$

$$\propto \sqrt{\frac{(2\ell+1)(\ell-2)!}{(\ell+2)!}} (\delta_{m2} + \delta_{m,-2}). \quad (\text{C3})$$

The contribution of this mode to the power spectrum is thus  $\propto \sum_m |z_{\ell m}|^2 / (2\ell+1) \propto (\ell-2)! / (\ell+2)!$ . Since this is a rotational invariant, the contribution of any Fourier mode in any direction (and of any magnitude), and of either polarization, is the same. From this we infer that  $C_\ell \propto (\ell-2)! / (\ell+2)!$ . The power spectra for the vector and scalar modes can be similarly obtained.

Likewise, the angular deflection from a wave propagating in the  $\hat{p}$  direction is [24]

$$(\delta n)^a(\hat{n}) = \frac{(n^a + p^a)n^b n^c h_{bc}}{2(1 + \hat{n} \cdot \hat{p})} - \frac{1}{2} n^b h_{ab}. \quad (\text{C4})$$

The scalar E-mode pattern associated with this is  $E(\hat{n}) = \nabla_a (\delta n)^a$ , while the B-mode pattern is  $B(\hat{n}) = \epsilon_{abc} n_a \nabla_b (\delta n)^c$ . Using  $\nabla_a n_b = \delta_{ab} - n_a n_b$  and  $\nabla_a (\hat{p} \cdot \hat{n}) = p_a - n_a (\hat{p} \cdot \hat{n})$ , we find

$$E(\hat{n}) = -\frac{1}{2} \text{Tr}h + \frac{(n^a + p^a)n^b h_{ab}}{1 + \hat{p} \cdot \hat{n}}, \quad (\text{C5})$$

and

$$Y_{(\ell m)a}^E(\Theta, \Phi) = -\frac{r}{\sqrt{\ell(\ell+1)}} \nabla_a Y_{\ell m}(\Theta, \Phi) = -\frac{1}{\sqrt{\ell(\ell+1)}} \left[ \hat{\theta}_a \frac{\partial}{\partial \Theta} + \hat{\phi}_a \frac{1}{\sin \Theta} \frac{\partial}{\partial \Phi} \right] Y_{\ell m}(\Theta, \Phi)$$

$$= -\frac{1}{2} \frac{1}{\sqrt{\ell(\ell+1)}} \left\{ \hat{\theta}_a [\sqrt{(\ell-m)(\ell+m+1)} e^{-i\Phi} Y_{\ell, m+1}(\Theta, \Phi) - \sqrt{(\ell+m)(\ell-m+1)} e^{i\Phi} Y_{\ell, m-1}(\Theta, \Phi)] \right.$$

$$\left. + \hat{\phi}_a \frac{2im}{\sin \Theta} Y_{\ell, m}(\cos \Theta) \right\}, \quad (\text{D1})$$

$$Y_{(\ell m)a}^B(\Theta, \Phi) = -\frac{r}{\sqrt{\ell(\ell+1)}} \epsilon_{abc} n^b \nabla^c Y_{\ell m}(\Theta, \Phi) = -\frac{1}{\sqrt{\ell(\ell+1)}} \left[ \hat{\phi}_a \frac{\partial}{\partial \Theta} - \hat{\theta}_a \frac{1}{\sin \Theta} \frac{\partial}{\partial \Phi} \right] Y_{\ell m}(\Theta, \Phi)$$

$$= -\frac{1}{2} \frac{1}{\sqrt{\ell(\ell+1)}} \left\{ \hat{\phi}_a [\sqrt{(\ell-m)(\ell+m+1)} e^{-i\Phi} Y_{\ell, m+1}(\Theta, \Phi) - \sqrt{(\ell+m)(\ell-m+1)} e^{i\Phi} Y_{\ell, m-1}(\Theta, \Phi)] \right.$$

$$\left. - \hat{\theta}_a \frac{2im}{\sin \Theta} Y_{\ell, m}(\cos \Theta) \right\}. \quad (\text{D2})$$

There is a third vector spherical harmonic  $Y_{(\ell m)a}^L(\Theta, \Phi)$  in the direction normal to the two-sphere of the sky, but it does not enter our calculations here. These vector spherical harmonics obey the orthogonality relation

$$\int d\hat{n} Y_{(\ell m)a}^X(\hat{n}) [Y_{(\ell' m')^a}^{X'}(\hat{n})]^* = \delta_{\ell\ell'} \delta_{mm'} \delta_{XX'}, \quad (\text{D3})$$

where  $X, X' = \{E, B, L\}$ .

$$B(\hat{n}) = \epsilon_{abc} \frac{p^a n^d n_c h_{bd}}{1 + \hat{p} \cdot \hat{n}}. \quad (\text{C6})$$

Now consider again the transverse-traceless gravitational wave propagating in the  $\hat{z}$  direction with + polarization. The transverse-traceless wave has  $\text{Tr}h = 0$  and  $p^a h_{ab} = 0$  from which we infer that the angular pattern of the E mode from transverse-traceless gravitational waves is identical with that for the redshift. This thus explains why the E-mode correlation function  $\beta^{EE}(\Theta)$  has the exact same form as the Hellings-Downs curve. It is furthermore found that the B-mode pattern is the same as the E-mode pattern, but rotated about  $\hat{p}$  by  $45^\circ$ , thus explaining why the B-mode correlation function and power spectrum are the same as those for the E mode (and also why it is not correlated with the redshift). The power spectra for the vector and scalar E and B modes are similarly derived.

#### APPENDIX D: RELATION BETWEEN DEFLECTION-ANGLE CORRELATION FUNCTIONS AND POWER SPECTRA

The correlation functions described in Sec. II A 1 are rotationally invariant. We can evaluate them most easily, though, by choosing one of the two points to be correlated to be at the north pole ( $\Theta = \Phi = 0$ ) and the other at a  $(\Theta, \Phi) = 0$ . In terms of the conventional scalar spherical harmonics,  $Y_{\ell m}(\Theta, \Phi)$ , the vector spherical harmonics are [31]

Evaluating the vector spherical harmonics at  $\Phi = 0$  gives

$$Y_{(\ell m)a}^E(\Theta, \Phi = 0) = -\frac{1}{2} \sqrt{\frac{1}{\ell(\ell+1)} \frac{2\ell+1}{4\pi} \frac{(\ell-m)!}{(\ell+m)!}} \left\{ \hat{\theta}_a [P_\ell^{m+1}(\cos \Theta) - (\ell+m)(\ell-m+1)P_\ell^{m-1}(\cos \Theta)] + \hat{\phi}_a \frac{2im}{\sin \Theta} P_\ell^m(\cos \Theta) \right\}, \quad (\text{D4})$$

$$Y_{(\ell m)a}^B(\Theta, \Phi = 0) = -\frac{1}{2} \sqrt{\frac{1}{\ell(\ell+1)} \frac{2\ell+1}{4\pi} \frac{(\ell-m)!}{(\ell+m)!}} \left\{ \hat{\theta}_a [P_\ell^{m+1}(\cos \Theta) - (\ell+m)(\ell-m+1)P_\ell^{m-1}(\cos \Theta)] - \hat{\phi}_a \frac{2im}{\sin \Theta} P_\ell^m(\cos \Theta) \right\}, \quad (\text{D5})$$

where we have expressed the scalar spherical harmonics,

$$Y_{\ell m}(\Theta, \Phi) = \sqrt{\frac{2\ell+1}{4\pi} \frac{(\ell-m)!}{(\ell+m)!}} P_\ell^m(\cos \Theta) e^{im\Phi}, \quad (\text{D6})$$

in terms of associated Legendre polynomials,  $P_\ell^m(\cos \Theta)$ . Further evaluating at  $\Theta = 0$  using Eq. (5.2) in Ref. [35] gives

$$Y_{(\ell m)a}^E(0, 0) = \frac{1}{2} \sqrt{\frac{2\ell+1}{4\pi}} [(\delta_{m1} - \delta_{m,-1})\hat{\theta}_a + i(\delta_{m1} + \delta_{m,-1})\hat{\phi}_a], \quad (\text{D7})$$

$$Y_{(\ell m)a}^B(0, 0) = \frac{1}{2} \sqrt{\frac{2\ell+1}{4\pi}} [(\delta_{m1} - \delta_{m,-1})\hat{\phi}_a - i(\delta_{m1} + \delta_{m,-1})\hat{\theta}_a]. \quad (\text{D8})$$

With these expressions, the correlation functions become,

$$\begin{aligned} C^{\parallel\parallel}(\Theta) &= \sum_{\ell m} [C_\ell^{EE} Y_{(\ell m)\theta}^E(\Theta, 0) Y_{(\ell m)\theta}^{E*}(0, 0) + C_\ell^{BB} Y_{(\ell m)\theta}^B(\Theta, 0) Y_{(\ell m)\theta}^{B*}(0, 0)] \\ &= \frac{1}{2} \sum_{\ell} \frac{2\ell+1}{4\pi} \left\{ C_\ell^{EE} \left[ P_\ell^0(\cos \Theta) - \frac{1}{\ell(\ell+1)} P_\ell^2(\cos \Theta) \right] - C_\ell^{BB} \frac{2}{\ell(\ell+1)} \frac{1}{\sin \Theta} P_\ell^1(\cos \Theta) \right\} \end{aligned} \quad (\text{D9})$$

$$\begin{aligned} C^{\perp\perp}(\Theta) &= \sum_{\ell m} [C_\ell^{EE} Y_{(\ell m)\phi}^E(\Theta, 0) Y_{(\ell m)\phi}^{E*}(0, 0) + C_\ell^{BB} Y_{(\ell m)\phi}^B(\Theta, 0) Y_{(\ell m)\phi}^{B*}(0, 0)] \\ &= \frac{1}{2} \sum_{\ell} \frac{2\ell+1}{4\pi} \left\{ -C_\ell^{EE} \frac{2}{\ell(\ell+1)} \frac{1}{\sin \Theta} P_\ell^1(\cos \Theta) + C_\ell^{BB} \left[ P_\ell^0(\cos \Theta) - \frac{1}{\ell(\ell+1)} P_\ell^2(\cos \Theta) \right] \right\}, \end{aligned} \quad (\text{D10})$$

while the cross-correlation function becomes

$$\begin{aligned} C^{\perp\parallel}(\Theta) &= \sum_{\ell m} [C_\ell^{EE} Y_{(\ell m)\phi}^E(\Theta, 0) Y_{(\ell m)\theta}^{E*}(0, 0) + C_\ell^{BB} Y_{(\ell m)\phi}^B(\Theta, 0) Y_{(\ell m)\theta}^{B*}(0, 0)] \\ &= -\frac{1}{2} \sum_{\ell} \frac{2\ell+1}{4\pi} C_\ell^{EB} \left[ \frac{1}{\ell(\ell+1)} P_\ell^2(\cos \Theta) - P_\ell^0(\cos \Theta) + \frac{2}{\ell(\ell+1)} \frac{1}{\sin \Theta} P_\ell^1(\cos \Theta) \right]. \end{aligned} \quad (\text{D11})$$

The  $z\parallel$  and  $z\perp$  correlations are analogously derived most simply by putting the deflection at the north pole and the redshift at  $(\Theta, 0)$ .

To write the power spectra in terms of the correlation functions, we define the vector quantities

$$\mathcal{C}_a(\Theta) \equiv C^{\parallel\parallel}(\Theta) \hat{\theta}_a + i C^{\perp\perp}(\Theta) \hat{\phi}_a = \sum_{\ell} \sqrt{\frac{2\ell+1}{4\pi}} [C_\ell^{EE} Y_{(\ell 1)a}^E(\Theta, 0) + i C_\ell^{BB} Y_{(\ell 1)a}^B(\Theta, 0)] \quad (\text{D12})$$

$$\mathcal{D}_a(\Theta) \equiv C^{\perp\parallel}(\Theta)(\hat{\theta}_a - i\hat{\phi}_a) = \sum_{\ell} \sqrt{\frac{2\ell+1}{4\pi}} C_{\ell}^{EB} [Y_{(\ell 1)a}^E(\Theta, 0) - iY_{(\ell 1)a}^B(\Theta, 0)]. \quad (\text{D13})$$

Using the orthogonality relation in Eq. (D3), which holds if the vector spherical harmonics are evaluated at  $\Phi = 0$ , the multipole moments are

$$C_{\ell}^{EE} = \sqrt{\frac{4\pi}{2\ell+1}} \int d\hat{n} C_a(\Theta) Y_{(\ell 1)}^{Ea}(\Theta, 0) \quad C_{\ell}^{BB} = -i \sqrt{\frac{4\pi}{2\ell+1}} \int d\hat{n} C_a(\Theta) Y_{(\ell 1)}^{Ba}(\Theta, 0), \quad (\text{D14})$$

and from these follow Eqs. (19) and (20). Similarly, for the cross-correlation,

$$C_{\ell}^{EB} = \frac{1}{2} \sqrt{\frac{4\pi}{2\ell+1}} \int d\hat{n} \mathcal{D}_a(\Theta) [Y_{(\ell 1)}^{Ea}(\Theta, 0) + iY_{(\ell 1)}^{Ba}(\Theta, 0)], \quad (\text{D15})$$

from which Eq. (21) follows. The inverse relations in Eq. (22) for the redshift-deflection cross-correlations follow from the orthogonality of the spherical harmonics.

- 
- [1] R. S. Foster and D. C. Backer, Constructing a pulsar timing array, *Astrophys. J.* **361**, 300 (1990).
- [2] G. Hobbs, The Parkes pulsar timing array, *Classical Quantum Gravity* **30**, 224007 (2013).
- [3] R. N. Manchester *et al.*, The parkes pulsar timing array project, *Pub. Astron. Soc. Aust.* **30**, e017 (2013).
- [4] Z. Arzoumanian *et al.* (NANOGrav Collaboration), The NANOGrav 11-year data set: Pulsar-timing constraints on the stochastic gravitational-wave background, *Astrophys. J.* **859**, 47 (2018).
- [5] L. Lentati *et al.*, European pulsar timing array limits on an isotropic stochastic gravitational-wave background, *Mon. Not. R. Astron. Soc.* **453**, 2576 (2015).
- [6] J. P. W. Verbiest *et al.*, The international pulsar timing array: First data release, *Mon. Not. R. Astron. Soc.* **458**, 1267 (2016).
- [7] S. L. Detweiler, Pulsar timing measurements and the search for gravitational waves, *Astrophys. J.* **234**, 1100 (1979).
- [8] M. V. Sazhin, Opportunities for detecting ultralong gravitational waves, *Sov. Astron.* **22**, 36 (1978).
- [9] R. W. Hellings and G. S. Downs, Upper limits on the isotropic gravitational radiation background from pulsar timing analysis, *Astrophys. J.* **265**, L39 (1983).
- [10] N. L. Zakamska and S. Tremaine, Constraints on the acceleration of the solar system from high-precision timing, *Astron. J.* **130**, 1939 (2005).
- [11] M. Rajagopal and R. W. Romani, Ultralow frequency gravitational radiation from massive black hole binaries, *Astrophys. J.* **446**, 543 (1995).
- [12] A. H. Jaffe and D. C. Backer, Gravitational waves probe the coalescence rate of massive black hole binaries, *Astrophys. J.* **583**, 616 (2003).
- [13] A. Sesana, Systematic investigation of the expected gravitational wave signal from supermassive black hole binaries in the pulsar timing band, *Mon. Not. R. Astron. Soc.* **433**, L1 (2013).
- [14] V. Ravi, J. S. B. Wyithe, R. M. Shannon, and G. Hobbs, Prospects for gravitational-wave detection and supermassive black hole astrophysics with pulsar timing arrays, *Mon. Not. R. Astron. Soc.* **447**, 2772 (2015).
- [15] L. Z. Kelley, L. Blecha, L. Hernquist, A. Sesana, and S. R. Taylor, The gravitational wave background from massive black hole binaries in illustris: Spectral features and time to detection with pulsar timing arrays, *Mon. Not. R. Astron. Soc.* **471**, 4508 (2017).
- [16] M. Maggiore, Gravitational wave experiments and early universe cosmology, *Phys. Rep.* **331**, 283 (2000).
- [17] S. Burke-Spolaor, Gravitational-wave detection and astrophysics with pulsar timing arrays, [arXiv:1511.07869](https://arxiv.org/abs/1511.07869).
- [18] A. N. Lommen, Pulsar timing arrays: The promise of gravitational wave detection, *Rep. Prog. Phys.* **78**, 124901 (2015).
- [19] G. Hobbs and S. Dai, A review of pulsar timing array gravitational wave research, [arXiv:1707.01615](https://arxiv.org/abs/1707.01615).
- [20] N. Yunes and X. Siemens, Gravitational-wave tests of general relativity with ground-based detectors and pulsar timing-arrays, *Living Rev. Relativity* **16**, 9 (2013).
- [21] V. B. Braginsky, N. S. Kardashev, I. D. Novikov, and A. G. Polnarev, Propagation of electromagnetic radiation in a random field of gravitational waves and space radio interferometry, *Nuovo Cimento B* **105**, 1141 (1990).
- [22] N. Kaiser and A. H. Jaffe, Bending of light by gravity waves, *Astrophys. J.* **484**, 545 (1997).
- [23] J. Darling, A. E. Truebenbach, and J. Paine, Astrometric limits on the stochastic gravitational wave background, *Astrophys. J.* **861**, 113 (2018).
- [24] L. G. Book and E. E. Flanagan, Astrometric effects of a stochastic gravitational wave background, *Phys. Rev. D* **83**, 024024 (2011).

- [25] C. J. Moore, D. Mihaylov, A. Lasenby, and G. Gilmore, Astrometric Search Method for Individually Resolvable Gravitational Wave Sources with Gaia, *Phys. Rev. Lett.* **119**, 261102 (2017).
- [26] D. P. Mihaylov, C. J. Moore, J. R. Gair, A. Lasenby, and G. Gilmore, Astrometric effects of gravitational wave backgrounds with non-Einsteinian polarizations, *Phys. Rev. D* **97**, 124058 (2018).
- [27] L. O’Beirne and N. J. Cornish, Constraining the polarization content of gravitational waves with astrometry, *Phys. Rev. D* **98**, 024020 (2018).
- [28] K. J. Lee, F. A. Jenet, and R. H. Price, Pulsar timing as a probe of non-Einsteinian polarizations of gravitational waves, *Astrophys. J.* **685**, 1304 (2008).
- [29] S. J. Chamberlin and X. Siemens, Stochastic backgrounds in alternative theories of gravity: Overlap reduction functions for pulsar timing arrays, *Phys. Rev. D* **85**, 082001 (2012).
- [30] C. Boehm *et al.* (Theia Collaboration), Theia: Faint objects in motion or the new astrometry frontier, [arXiv:1707.01348](https://arxiv.org/abs/1707.01348).
- [31] L. Dai, M. Kamionkowski, and D. Jeong, Total angular momentum waves for scalar, vector, and tensor fields, *Phys. Rev. D* **86**, 125013 (2012).
- [32] L. Dai, D. Jeong, and M. Kamionkowski, Wigner-Eckart theorem in cosmology: Bispectra for total-angular-momentum waves, *Phys. Rev. D* **87**, 043504 (2013).
- [33] M. Kamionkowski, Circular polarization in a spherical basis, *Phys. Rev. D* **97**, 123529 (2018).
- [34] J. R. Gair, J. D. Romano, and S. R. Taylor, Mapping gravitational-wave backgrounds of arbitrary polarization using pulsar timing arrays, *Phys. Rev. D* **92**, 102003 (2015).
- [35] M. Kamionkowski, A. Kosowsky, and A. Stebbins, Statistics of cosmic microwave background polarization, *Phys. Rev. D* **55**, 7368 (1997).
- [36] S. R. Taylor *et al.*, Limits on Anisotropy in the Nanohertz Stochastic Gravitational-Wave Background, *Phys. Rev. Lett.* **115**, 041101 (2015).
- [37] C. M. F. Mingarelli *et al.*, The local nanohertz gravitational-wave landscape from supermassive black hole binaries, *Nat. Astron.* **1**, 886 (2017).
- [38] M. Kamionkowski, L. Dai, and D. Jeong, Tensor-induced B modes with no temperature fluctuations, *Phys. Rev. D* **89**, 107302 (2014).
- [39] M. Maggiore, *Gravitational Waves, Volume II: Astrophysics and Cosmology* (Oxford University Press, Oxford, 2018).
- [40] G. Hobbs *et al.*, Development of a pulsar-based time-scale, *Mon. Not. R. Astron. Soc.* **427**, 2780 (2012).
- [41] M. Isi and L. C. Stein, Measuring stochastic gravitational-wave energy beyond general relativity, *Phys. Rev. D* **98**, 104025 (2018).
- [42] D. M. Eardley, D. L. Lee, and A. P. Lightman, Gravitational-wave observations as a tool for testing relativistic gravity, *Phys. Rev. D* **8**, 3308 (1973).
- [43] D. Liang, Y. Gong, S. Hou, and Y. Liu, Polarizations of gravitational waves in  $f(R)$  gravity, *Phys. Rev. D* **95**, 104034 (2017).
- [44] S. Hou, Y. Gong, and Y. Liu, Polarizations of gravitational waves in Horndeski theory, *Eur. Phys. J. C* **78**, 378 (2018).
- [45] C. Caprini and D. G. Figueroa, Cosmological backgrounds of gravitational waves, *Classical Quantum Gravity* **35**, 163001 (2018).
- [46] M. Enoki and M. Nagashima, The effect of orbital eccentricity on gravitational wave background radiation from supermassive black hole binaries, *Prog. Theor. Phys.* **117**, 241 (2007).
- [47] A. Sesana, A. Vecchio, and C. N. Colacino, The stochastic gravitational-wave background from massive black hole binary systems: Implications for observations with Pulsar Timing Arrays, *Mon. Not. R. Astron. Soc.* **390**, 192 (2008).
- [48] P. Amaro-Seoane, A. Sesana, L. Hoffman, M. Benacquista, C. Eichhorn, J. Makino, and R. Spurzem, Triplets of supermassive black holes: astrophysics, gravitational waves and detection, *Mon. Not. R. Astron. Soc.* **402**, 2308 (2010).
- [49] A. Sesana, A. Vecchio, and M. Volonteri, Gravitational waves from resolvable massive black hole binary systems and observations with Pulsar Timing Arrays, *Mon. Not. R. Astron. Soc.* **394**, 2255 (2009).
- [50] L. Boyle and U. L. Pen, Pulsar timing arrays as imaging gravitational wave telescopes: Angular resolution and source (de)confusion, *Phys. Rev. D* **86**, 124028 (2012).
- [51] P. A. Rosado, A. Sesana, and J. Gair, Expected properties of the first gravitational wave signal detected with pulsar timing arrays, *Mon. Not. R. Astron. Soc.* **451**, 2417 (2015).
- [52] R. Kato and J. Soda, Probing circular polarization in stochastic gravitational wave background with pulsar timing arrays, *Phys. Rev. D* **93**, 062003 (2016).
- [53] T. L. Smith and R. Caldwell, Sensitivity to a frequency-dependent circular polarization in an isotropic stochastic gravitational wave background, *Phys. Rev. D* **95**, 044036 (2017).
- [54] A. Hajian and T. Souradeep, Measuring statistical isotropy of the CMB anisotropy, *Astrophys. J.* **597**, L5 (2003).
- [55] L. G. Book, M. Kamionkowski, and T. Souradeep, Odd-parity bipolar spherical harmonics, *Phys. Rev. D* **85**, 023010 (2012).
- [56] C. M. F. Mingarelli, T. Sidery, I. Mandel, and A. Vecchio, Characterizing gravitational wave stochastic background anisotropy with pulsar timing arrays, *Phys. Rev. D* **88**, 062005 (2013).
- [57] C. Conneely, A. H. Jaffe, and C. M. F. Mingarelli, On the amplitude and stokes parameters of a stochastic gravitational-wave background, [arXiv:1808.05920](https://arxiv.org/abs/1808.05920).
- [58] D. Jeong and M. Kamionkowski, Clustering Fossils from the Early Universe, *Phys. Rev. Lett.* **108**, 251301 (2012).
- [59] E. Roebber and G. Holder, Harmonic space analysis of pulsar timing array redshift maps, *Astrophys. J.* **835**, 21 (2017).